Evolution of a short surface wave on a very long surface wave of finite amplitude

By MAMOUN NACIRI and CHIANG C. MEI

Ralph M. Parsons Laboratory, Department of Civil Engineering, Massachusetts Institute of Technology, Cambridge, MA 02139, USA

To facilitate the theoretical prediction of the evolution of a short gravity wave on a long wave of finite amplitude, we consider a model where the long wave is represented by Gerstner's exact but rotational solution in Lagrangian coordinates. Analytical formulae for the modulation of an infinitesimal irrotational short wave are shown to be qualitatively accurate in comparison with the numerical results by Longuet-Higgins (1987) and with the analytical results by Henyey *et al.* (1988) for irrotational long waves. Discrepancies are generally of second order in the long-wave steepness, consistent with the vorticity in Gerstner's solution. Weakly nonlinear short waves are shown to be parametrically excited by the long wave over a long time. In particular, multiple bands of modulational instability appear in the parameter space. Numerical calculations of the nonlinear evolution equation show the onset of chaos for sufficiently large parameter $\alpha = \epsilon(k\bar{A})^2/(2\Omega/\sigma)$, where $\epsilon k\bar{A}$ is the short-wave steepness and $(\epsilon\Omega, \sigma)$ the frequency of the (long, short) wave. Furthermore, if the short-wave amplitude A is approximated by a two-mode truncated Fourier series, the evolution equation reduces to a non-autonomous Hamiltonian system. The numerical solutions confirm that the onset of chaos is an inherent feature of the parametrically excited nonlinear system.

1. Introduction

The exchange of energy among waves of different lengths is an important dynamical process on the surface of the ocean. Recent stimulus for studying this topic stems from the fact that radar waves Bragg-scattered by the sea surface are in the typical range from a few centimeters (X-band) to a few tens of centimetres (L-band). Proper interpretation of the SAR images for large-scale surface features requires sound knowledge of the hydrodynamic interaction between short and long scales, particularly between short surface waves of $O(1\text{–}10)$ cm and long surface waves of $O(10\text{–}1000)$ m.

Longuet-Higgins & Stewart (1960) first developed a theory on the weak interaction between a train of short waves and a train of long waves, both of which had low amplitudes. They deduced simple formulae showing the shortening and steepening of short waves when the long-wave crests pass beneath them. More recently Longuet-Higgins (1987) considered the case where the long wave is an irrotational Stokes wave of finite amplitude up to the maximum height. By an efficient numerical algorithm the long wave is first calculated. The modulation of the short wave during the passage of a few long wave crests is found to be considerably enhanced by the long wave. Henyey *et al.* (1988) have developed a theory for the linearized evolution of short waves on a general two-dimensional long-wave field. Assuming irrotational

flow, they employed a Hamiltonian formulation and deduced the action conservation law for the short waves. Numerically, Kharif (1990) has shown that Longuet-Higgins' calculations can be alternatively obtained by considering the stability of long waves subjected to superharmonic perturbations. Zhang & Melville (1900) have extended these calculations and further deduced the slow modulation equation of Schrödinger form for the envelope of a weakly nonlinear short wave. With the coefficients obtained from the numerical solution of the long wave, short waves which remain steady along the long wave profile were computed.

As is known for a single wave train in calm sea, the long-term evolution after the initial stage of Benjamin–Feir (sideband) instability involves a complex interplay between nonlinearity and dispersion. The short-wave envelope undergoes recursive transitions due to the energy exchange between the unstable sidebands and the carrier wave. Owing to the long wave, the short wave is in an apparent gravity field oscillatory in time, hence is further subjected to parametric excitation. Since simple nonlinear oscillations under similar excitation are known to respond chaotically, it is interesting to examine whether and how chaos can appear in the short waves. To facilitate theoretical calculations and physical deductions, we have chosen to model the long wave by Gerstner's simple and exact solution in Lagrangian coordinates. Admittedly, Gerstner's wave possesses finite vorticity of a special form and has a free-surface profile differing noticeably from the irrotational theory of Stokes, if the steepnes is sufficiently great. But the maximum vorticity at the free surface is proportional to the square of the long-wave steepness KB and need not be very large for moderate steepness, say $KB \leqslant 0.3$. Physical deductions may still be reasonable with a considerable gain in analytical simplicity.

In this paper we shall first show that Longuet-Higgins's (1987) numerical results on the modulation of infinitesimal short waves on a long Stokes wave can be qualitatively well reproduced by explicit formulae for a Gerstner's wave with $KB < 0.4$ (according to the irrotational theory, the maximum steepness is $KB \approx 0.4432$). Agreement with the irrotational theory by Henyey *et al.* (1988) is also within $O(K^2B^2)$ at least, which is comparable to the vorticity difference in the long waves. The asymptotic equation governing the nonlinear evolution of a slowly modulated short-wave envelope is deduced with all its coefficients given explicitly in terms of the long wave. The solution for a short Stokes wave riding on a long wave is now simple. By applying Floquet theory, the linearized instability of sidebands is calculated, showing the emergence of new unstable bands when the parameter α increases. Numerical results for a broad range of α are discussed for the post-instability evolution of the short-wave envelope when disturbed by the most unstable sidebands. Evidence of chaos is found where α is sufficiently large. To give further insight into the inherent tendency toward chaos we study a truncated non-autonomous dynamical system involving just two unstable modes (the carrier waves and the sidebands). The numerical results confirm the general trend toward chaos. Thus wave/wave interactions appear to be a powerful deterministic cause contributing to the random appearance of the ocean surface.

2. Exact and perturbation equations in Lagrangian coordinates

In the Lagrangian description, the dependent variables are the coordinates (X, Z) of the instantaneous position of a particle, while the independent variables are time

and two parameters (a, c) characterizing the particle, such as its initial position. For two-dimensional problems, the continuity equation reads

$$J(a, c, t) = \frac{\partial X}{\partial a}\frac{\partial Z}{\partial c} - \frac{\partial X}{\partial c}\frac{\partial Z}{\partial a} = J(a, c, 0). \tag{2.1}$$

The Jacobian J reduces to unity if (a, c) represents the initial position. Constancy of vorticity gives

$$\frac{\partial \zeta}{\partial t} = 0, \quad \text{where} \quad \zeta = \frac{1}{J}\left\{\frac{\partial X}{\partial a}\frac{\partial^2 X}{\partial c\,\partial t} - \frac{\partial X}{\partial c}\frac{\partial^2 X}{\partial a\,\partial t} + \frac{\partial Z}{\partial a}\frac{\partial^2 Z}{\partial c\,ct} - \frac{\partial Z}{\partial c}\frac{\partial^2 Z}{\partial a\,\partial t}\right\}. \tag{2.2a, b}$$

On the free surface designated by $c = 0$, the pressure is assumed to vanish

$$\frac{\partial X}{\partial a}\frac{\partial^2 X}{\partial t^2} + \frac{\partial Z}{\partial a}\left(g + \frac{\partial^2 Z}{\partial t^2}\right) = 0, \quad c = 0, \tag{2.3}$$

where g is the gravitational acceleration.

We now define the Lagrangian particle displacements (x, z) by

$$X(a, c, t) = a + x(a, c, t), \quad Z(a, c, t) = c + z(a, c, t). \tag{2.4}$$

Equations (2.1)–(2.3) become respectively

$$1 + \frac{\partial x}{\partial a} + \frac{\partial z}{\partial c} + \frac{\partial x}{\partial a}\frac{\partial z}{\partial c} - \frac{\partial x}{\partial c}\frac{\partial z}{\partial a} = J, \tag{2.5}$$

$$\frac{\partial^3 x}{\partial c\,\partial t^2}\left\{1 + \frac{\partial x}{\partial a}\right\} - \frac{\partial^3 z}{\partial a\,\partial t^2}\left\{1 + \frac{\partial z}{\partial c}\right\} - \frac{\partial^3 x}{\partial a\,\partial t^2}\frac{\partial x}{\partial c} + \frac{\partial^3 z}{\partial c\,\partial t^2}\frac{\partial z}{\partial a} = 0 \tag{2.6}$$

and

$$\frac{\partial^2 x}{\partial t^2} + g\frac{\partial z}{\partial a} + \frac{\partial x}{\partial a}\frac{\partial^2 x}{\partial t^2} + \frac{\partial z}{\partial a}\frac{\partial^2 z}{\partial t^2} = 0, \quad c = 0. \tag{2.7}$$

As $c \rightarrow -\infty$, the displacements diminish to zero.

Let us consider two trains of deep-water waves with one very much shorter than the other. Omitting the formality of normalization, we use the wavenumber k and frequency σ of the short wave as the basic space- and timescales. Let $\epsilon \ll 1$ be a small ordering parameter. We shall assume specifically that the wavenumber, the intrinsic frequency, and the amplitude of the short wave at the leading order are $\{k, \sigma, \epsilon A\}$ and the corresponding quantities of the exact long wave are $\{\epsilon^2 K, \epsilon\Omega, B/\epsilon^2\}$, where k, σ, A, K, Ω and B are all regarded as being $O(1)$. In this problem the short wave is expected to be modulated either by interaction with the long wave, or by its own nonlinearity, while the long wave is assumed to be uniform in space and time. Let the following multiple-scale coordinates and times be introduced:

$$(a_j, c_j, t_j) = \epsilon^j(a, c, t), \quad j = 1, 2. \tag{2.8}$$

In view of the scale assumptions, the Lagrangian displacements can be expanded in perturbation series as follows:

$$\begin{aligned} x &= \epsilon^{-2}x_{-2} + \epsilon x_1 + \epsilon^2 x_2 + \epsilon^3 x_3 + O(\epsilon^4), \\ z &= \epsilon^{-2}z_{-2} + \epsilon z_1 + \epsilon^2 z_2 + \epsilon^3 z_3 + O(\epsilon^4), \end{aligned}\left.\right\} \tag{2.9}$$

where x_{-2} and z_{-2} represent long-wave displacements, which depend only on (a_2, c_2, t_1). The remaining terms correspond to short waves and may depend on all

scales. Upon introducing (2.9) in (2.5)–(2.7), and collecting terms of similar order in ϵ, we obtain the following sequence of governing equations.

$O(1)$:

Continuity

$$1+\frac{\partial x_{-2}}{\partial a_2}+\frac{\partial z_{-2}}{\partial c_2}+\frac{\partial x_{-2}}{\partial a_2}\frac{\partial z_{-2}}{\partial c_2}-\frac{\partial x_{-2}}{\partial c_2}\frac{\partial z_{-2}}{\partial a_2}=J, \tag{2.10a}$$

Free-surface boundary condition

$$\frac{\partial^2 x_{-2}}{\partial t_1^2}\left\{1+\frac{\partial x_{-2}}{\partial a_2}\right\}+\frac{\partial z_{-2}}{\partial a_2}\left\{g+\frac{\partial^2 z_{-2}}{\partial t_1^2}\right\}=0, \quad c=0. \tag{2.10b}$$

Both of these equations involve only long-wave displacements. The vorticity equation has no contribution at this order.

$O(\epsilon)$:

Continuity

$$\frac{\partial x_1}{\partial a}+\frac{\partial z_1}{\partial c}+\frac{\partial x_{-2}}{\partial a_2}\frac{\partial z_1}{\partial c}-\frac{\partial x_{-2}}{\partial c_2}\frac{\partial z_1}{\partial a}-\frac{\partial z_{-2}}{\partial a_2}\frac{\partial x_1}{\partial c}+\frac{\partial z_{-2}}{\partial c_2}\frac{\partial x_1}{\partial a}=0, \tag{2.11a}$$

Vorticity

$$\frac{\partial^3 x_1}{\partial c\,\partial t^2}-\frac{\partial^3 z_1}{\partial a\,\partial t^2}+\frac{\partial z_{-2}}{\partial a_2}\frac{\partial^3 z_1}{\partial c\,\partial t^2}-\frac{\partial z_{-2}}{\partial c_2}\frac{\partial^3 z_1}{\partial a\,\partial t^2}+\frac{\partial x_{-2}}{\partial a_2}\frac{\partial^3 x_1}{\partial c\,\partial t^2}-\frac{\partial x_{-2}}{\partial c_2}\frac{\partial^3 x_1}{\partial a\,\partial t^2}=0, \tag{2.11b}$$

Free-surface boundary condition

$$\frac{\partial^2 x_1}{\partial t^2}+g\frac{\partial z_1}{\partial a}+\frac{\partial z_{-2}}{\partial a_2}\frac{\partial^2 z_1}{\partial t^2}+\frac{\partial^2 z_{-2}}{\partial t_1^2}\frac{\partial z_1}{\partial a}+\frac{\partial x_{-2}}{\partial a_2}\frac{\partial^2 x_1}{\partial t^2}+\frac{\partial^2 x_{-2}}{\partial t_1^2}\frac{\partial x_1}{\partial a}=0, \quad c=0. \tag{2.11c}$$

$O(\epsilon^2)$:

Continuity

$$\frac{\partial x_2}{\partial a}+\frac{\partial z_2}{\partial c}+\frac{\partial x_1}{\partial a_1}+\frac{\partial z_1}{\partial c_1}+\frac{\partial x_{-2}}{\partial a_2}\frac{\partial z_2}{\partial c}-\frac{\partial x_{-2}}{\partial c_2}\frac{\partial z_2}{\partial a}-\frac{\partial z_{-2}}{\partial a_2}\frac{\partial x_2}{\partial c}+\frac{\partial z_{-2}}{\partial c_2}\frac{\partial x_2}{\partial a}+\frac{\partial x_1}{\partial a}\frac{\partial z_1}{\partial c}-\frac{\partial x_1}{\partial c}\frac{\partial z_1}{\partial a}$$

$$+\frac{\partial x_{-2}}{\partial a_2}\frac{\partial z_1}{\partial c_1}-\frac{\partial x_{-2}}{\partial c_2}\frac{\partial z_1}{\partial a_1}-\frac{\partial z_{-2}}{\partial a_2}\frac{\partial x_1}{\partial c_1}+\frac{\partial z_{-2}}{\partial c_2}\frac{\partial x_1}{\partial a_1}=0, \tag{2.12a}$$

Vorticity

$$\frac{\partial^3 x_{-2}}{\partial t_1^2\,\partial c_2}-\frac{\partial^3 z_{-2}}{\partial t_1^2\,\partial a_2}-\frac{\partial^3 z_{-2}}{\partial t_1^2\,\partial a_2}\frac{\partial z_{-2}}{\partial c_2}+\frac{\partial^3 z_{-2}}{\partial t_1^2\,\partial c_2}\frac{\partial z_{-2}}{\partial a_2}-\frac{\partial^3 x_{-2}}{\partial t_1^2\,\partial a_2}\frac{\partial x_{-2}}{\partial c_2}$$

$$+\frac{\partial^3 x_{-2}}{\partial t_1^2\,\partial c_2}\frac{\partial x_{-2}}{\partial a_2}+\frac{\partial^3 x_2}{\partial c\,\partial t^2}-\frac{\partial^3 z_2}{\partial a\,\partial t^2}+2\frac{\partial^3 x_1}{\partial t_1\,\partial c\,\partial t}-2\frac{\partial^3 z_1}{\partial t_1\,\partial a\,\partial t}+\frac{\partial^3 x_1}{\partial c_1\,\partial t^2}-\frac{\partial^3 z_1}{\partial a_1\,\partial t^2}$$

$$+\frac{\partial x_{-2}}{\partial a_2}\frac{\partial^3 x_2}{\partial c\,\partial t^2}-\frac{\partial x_{-2}}{\partial c_2}\frac{\partial^3 x_2}{\partial a\,\partial t^2}+\frac{\partial x_1}{\partial a}\frac{\partial^3 x_1}{\partial c\,\partial t^2}-\frac{\partial^3 x_1}{\partial a\,\partial t^2}\frac{\partial x_1}{\partial c}$$

$$+2\frac{\partial x_{-2}}{\partial a_2}\frac{\partial^3 x_1}{\partial t_1\,\partial c\,\partial t}-2\frac{\partial x_{-2}}{\partial c_2}\frac{\partial^3 x_1}{\partial t_1\,\partial a\,\partial t}+\frac{\partial x_{-2}}{\partial a_2}\frac{\partial^3 x_1}{\partial c_1\,\partial t^2}-\frac{\partial x_{-2}}{\partial c_2}\frac{\partial^3 x_1}{\partial a_1\,\partial t^2}$$

$$+\frac{\partial z_{-2}}{\partial a_2}\frac{\partial^3 z_2}{\partial c\,\partial t^2}-\frac{\partial z_{-2}}{\partial c_2}\frac{\partial^3 z_2}{\partial a\,\partial t^2}+\frac{\partial z_1}{\partial a}\frac{\partial^3 z_1}{\partial c\,\partial t^2}-\frac{\partial^3 z_1}{\partial a\,\partial t^2}\frac{\partial z_1}{\partial c}$$

$$+2\frac{\partial z_{-2}}{\partial a_2}\frac{\partial^3 z_1}{\partial t_1\,\partial c\,\partial t}-2\frac{\partial z_{-2}}{\partial c_2}\frac{\partial^3 z_1}{\partial t_1\,\partial a\,\partial t}+\frac{\partial z_{-2}}{\partial a_2}\frac{\partial^3 z_1}{\partial c_1\,\partial t^2}-\frac{\partial z_{-2}}{\partial c_2}\frac{\partial^3 z_1}{\partial a_1\,\partial t^2}=0, \tag{2.12b}$$

Free-surface boundary condition

$$\frac{\partial^2 x_2}{\partial t^2} + g\frac{\partial z_2}{\partial a} + 2\frac{\partial^2 x_1}{\partial t_1 \partial t} + g\frac{\partial z_1}{\partial a_1} + \frac{\partial x_{-2}}{\partial a_2}\frac{\partial^2 x_2}{\partial t^2} + \frac{\partial^2 x_{-2}}{\partial t_1^2}\frac{\partial x_2}{\partial a}$$

$$+ \frac{\partial x_1}{\partial a}\frac{\partial^2 x_1}{\partial t^2} + 2\frac{\partial x_{-2}}{\partial a_2}\frac{\partial^2 x_1}{\partial t_1 \partial t} + \frac{\partial^2 x_{-2}}{\partial t_1^2}\frac{\partial x_1}{\partial a_1} + \frac{\partial z_{-2}}{\partial a_2}\frac{\partial^2 z_2}{\partial t^2}$$

$$+ \frac{\partial^2 z_{-2}}{\partial t_1^2}\frac{\partial z_2}{\partial a} + \frac{\partial z_1}{\partial a}\frac{\partial^2 z_1}{\partial t^2} + 2\frac{\partial z_{-2}}{\partial a_2}\frac{\partial^2 z_1}{\partial t_1 \partial t} + \frac{\partial^2 z_{-2}}{\partial t_1^2}\frac{\partial z_1}{\partial a_1} = 0, \quad c = 0. \quad (2.12c)$$

The $O(\epsilon^3)$ governing equations are lengthy and may be found in Appendix A.

3. The long wave of Gerstner

Since the long waves are not affected at the leading order by the short waves, we set the part involving only x_{-2} and z_{-2} of the vorticity equation $(2.12b)$ to zero, i.e.

$$\frac{\partial^3 x_{-2}}{\partial c_2 \partial t_1^2}\left\{1 + \frac{\partial x_{-2}}{\partial a_2}\right\} - \frac{\partial^3 z_{-2}}{\partial a_2 \partial t_1^2}\left\{1 + \frac{\partial z_{-2}}{\partial c_2}\right\} + \frac{\partial z_{-2}}{\partial a_2}\frac{\partial^3 z_{-2}}{\partial c_2 \partial t_1^2} - \frac{\partial^3 x_{-2}}{\partial a_2 \partial t_1^2}\frac{\partial x_{-2}}{\partial c_2} = 0 \quad (3.1)$$

for $c < 0$. This equation and $(2.10a, b)$ admit the exact solution derived by Gerstner (1802) (a thorough discussion in English is available in Kochin, Kibel & Roze 1965):

$$x_{-2} = B\sin\phi\,\mathrm{e}^{Kc_2}, \quad z_{-2} = B\cos\phi\,\mathrm{e}^{Kc_2}, \quad (3.2a,b)$$

where the phase ϕ is defined as

$$\phi = \Omega t_1 - Ka_2 \quad \text{with} \quad \Omega^2 = gK. \quad (3.2c,d)$$

Alternatively, the long-wave solution is

$$X_2 = a_2 + B\sin\phi\,\mathrm{e}^{Kc_2}, \quad Z_2 = c_2 + B\cos\phi\,\mathrm{e}^{Kc_2}. \quad (3.3a,b)$$

Substitution of (3.3) into $(2.10a)$ yields

$$J = 1 - K^2 B^2\,\mathrm{e}^{2Kc_2}, \quad (3.4)$$

which is independent of time. It is well known that Gerstner's wave has a finite vorticity

$$\zeta = \epsilon\frac{-2\Omega K^2 B^2\,\mathrm{e}^{2Kc_2}}{1 - K^2 B^2\,\mathrm{e}^{2Kc_2}} \quad (3.5)$$

which is greatest on the free surface and decays exponentially with depth.

The free-surface elevation for Gerstner's wave is obtained by elevating $(3.3b)$ at $c_2 = 0$:

$$Z_2 = B\cos\phi. \quad (3.6a)$$

Upon defining the Eulerian phase as $\phi_E \equiv \Omega t_1 - KX_2$, we can derive from $(3.3a)$

$$\phi_E = \phi - KB\sin\phi \quad (3.6b)$$

Equations $(3.6a, b)$ define parametrically the free-surface elevation of Gerstner's wave.

It is also known (Kochin *et al.* 1965) that the mean vertical position of a fluid particle is

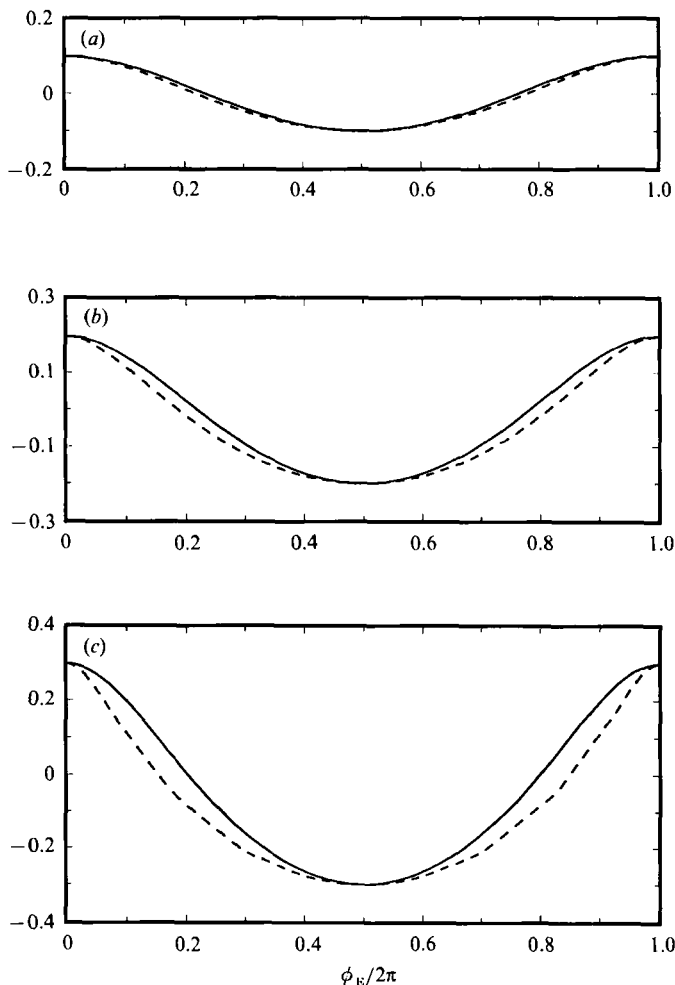$$\bar{Z}_2 = c_2 - \tfrac{1}{2}KB^2\,\mathrm{e}^{2Kc_2}. \quad (3.7)$$

FIGURE 1. Comparison of Gertsner (——) and Stokes (– – –) wave profiles for (a) $KB = 0.1$, (b) 0.2 and (c) 0.3.

Hence the mean sea level is at $\bar{Z}_2 = -\frac{1}{2}KB^2$, and the zero-crossings are located at

$$\cos \phi_{\text{crossing}} = -\frac{1}{2}KB. \tag{3.8}$$

For small KB, (3.8) admits two solutions in the interval $[0, 2\pi]$:

$$\phi_{\text{crossing}} \approx \tfrac{1}{2}\pi + \tfrac{1}{2}KB, \quad \text{or} \quad \tfrac{3}{2}\pi - \tfrac{1}{2}KB. \tag{3.9}$$

The corresponding Eulerian phase ϕ_E at the zero crossing can be readily found from (3.6b). For small KB, we get

$$\phi_{\text{E crossing}} \approx \tfrac{1}{2}\pi - \tfrac{1}{2}KB, \quad \text{or} \quad \tfrac{3}{2}\pi + \tfrac{1}{2}KB. \tag{3.10}$$

We compare in figure 1 the Stokes wave profiles computed from the very accurate series solution by Schwartz (1974) with Gerstner's wave profiles for $KB = 0.1, 0.2$ and 0.3. The agreement for $KB = 0.1$ is excellent while the differences become noticeable for $KB = 0.2$ and 0.3. From Schwartz (1974) the zero-crossing points of the Stokes wave are deduced to $O(K^5B^5)$ accuracy in Appendix B, with the result

$$\phi_{\text{E crossing}} = \tfrac{1}{2}\pi - \tfrac{3}{2}KB + \tfrac{29}{48}K^3B^3 + \tfrac{5743}{11520}K^5B^5 + O(K^7B^7). \tag{3.11}$$

Note that the difference from Gerstner's theory (3.9) is $O(KB)$ and relatively large.

4. Evolution equations for an irrotational short wave

4.1. *Short waves at the leading order*

Upon using (3.2) for Gerstner's wave in (2.11 a, b) and keeping $O(\epsilon)$ terms, we obtain from the continuity and vorticity equations

$$\{1+KB\cos\phi\}\frac{\partial x_1}{\partial a}+\{1-KB\cos\phi\}\frac{\partial z_1}{\partial c}-KB\sin\phi\left\{\frac{\partial x_1}{\partial c}+\frac{\partial z_1}{\partial a}\right\}=0 \qquad (4.1\,a)$$

and

$$\{1-KB\cos\phi\}\frac{\partial^3 x_1}{\partial c\,\partial t^2}-\{1+KB\cos\phi\}\frac{\partial^3 z_1}{\partial a\,\partial t^2}-KB\sin\phi\left\{\frac{\partial^3 x_1}{\partial a\,\partial t^2}-\frac{\partial^3 z_1}{\partial c\,\partial t^2}\right\}=0. \quad (4.1\,b)$$

The dynamic free-surface boundary condition (2.11 c) becomes

$$\{1-KB\cos\phi\}\left\{\frac{\partial^2 x_1}{\partial t^2}+g\frac{\partial z_1}{\partial a}\right\}+KB\sin\phi\left\{\frac{\partial^2 z_1}{\partial t^2}-g\frac{\partial x_1}{\partial a}\right\}=0, \quad c=0, \qquad (4.1\,c)$$

where use has been made of (3.2 c) and the dispersion relation (3.2 d). Let the solution for first-order displacements take the following form:

$$\binom{x_1}{z_1}=\binom{x_{10}}{z_{10}}+\binom{\mathrm{i}x^{11}}{z_{11}}\mathrm{e}^{\mathrm{i}(ka-\sigma t)} \qquad (4.2)$$

where x_{10}, z_{10}, x_{11} and z_{11} are unknown functions of c and of the slow coordinates a_1, a_2, t_1 and t_2. Denoting

$$V=\binom{x_{11}}{z_{11}} \qquad (4.3)$$

we get from (4.1 a, b) a set of first-order homogeneous differential equations

$$\boldsymbol{M}\frac{\partial V}{\partial c}=k\boldsymbol{N}V, \qquad (4.4\,a)$$

where $\boldsymbol{M}$ and $\boldsymbol{N}$ are the following matrices:

$$\boldsymbol{M}=\begin{pmatrix}-\mathrm{i}KB\sin\phi & 1-KB\cos\phi \\ 1-KB\cos\phi & -\mathrm{i}KB\sin\phi\end{pmatrix}, \quad \boldsymbol{N}=\begin{pmatrix}1+KB\cos\phi & \mathrm{i}KB\sin\phi \\ \mathrm{i}KB\sin\phi & 1+KB\cos\phi\end{pmatrix}.$$
$$(4.4\,b,\,c)$$

The solution that diminishes to zero at $c\rightarrow-\infty$ is

$$V=A\binom{1}{1}\mathrm{e}^{(\kappa_r+\mathrm{i}\kappa_i)c}, \qquad (4.5)$$

where $A(a_1,a_2,t_1,t^2)$ is the amplitude of the short wave and

$$\kappa_r=\frac{k(1-K^2B^2)}{1-2KB\cos\phi+K^2B^2}, \quad \kappa_i=\frac{2kKB\sin\phi}{1-2KB\cos\phi+K^2B^2}. \qquad (4.6\,\mathrm{a,\,b})$$

Both κ_r and κ_i depend on a_2 and t_1 through the long-wave phase ϕ. The imaginary part κ_i corresponds to the vertical component of the Lagrangian wavenumber associated with the following phase function $\tilde{S}$:

$$\tilde{S}=ka+\kappa_i c-\sigma t. \qquad (4.7)$$

The free-surface dynamic boundary condition (4.1 c) then yields

$$\sigma^2 = gk. \tag{4.8}$$

Thus in Lagrangian coordinates, the dispersion relation of the short waves is of the same form as that of the long wave, and does not depend *explicitly* on long-wave quantities. However, this does not remain so in the Eulerian coordinates, as will be shown later.

4.2. *General perturbation equations*

The solution at $O(\epsilon^j)$ can be expanded in the following general form:

$$x_j = x_{j0}(a_1, c, t_1) + \tfrac{1}{2}\mathrm{i} \sum_{l=1}^{j} x_{jl}(a_1, c, t_1)\,\mathrm{e}^{\mathrm{i}l(ka-\sigma t)} + \text{c.c.}, \quad j = 1, 2, 3, \ldots, \tag{4.9a}$$

$$z_j = z_{j0}(a_1, c, t_1) + \frac{1}{2} \sum_{l=1}^{j} z_{jl}(a_1, c, t_1)\,\mathrm{e}^{\mathrm{i}l(ka-\sigma t)} + \text{c.c.}, \quad j = 1, 2, 3, \ldots, \tag{4.9b}$$

where the displacement amplitudes x_{jl} and z_{jl} depend on c, a_1, a_2 and t_1. After substituting (4.9) in the continuity and vorticity equations, we separate the orders and harmonics to get the following typical non-homogeneous ordinary matrix differential equation:

$$\boldsymbol{M}\frac{\partial \boldsymbol{U}}{\partial c} = lk\boldsymbol{N}\boldsymbol{U} + \begin{pmatrix} F_{jl} \\ G_{jl} \end{pmatrix}, \tag{4.10a}$$

where $\boldsymbol{U} = (x_{jl}, z_{jl})^{\mathrm{T}}$ for $j = 1, 2, \ldots$ and $l = 1, \ldots, j$. With the dispersion relations for both short and long waves, the free-surface boundary condition takes the simple form

$$\left. \begin{aligned} (1 - KB\cos\phi)\,[lx_{jl} - z_{jl}] + \mathrm{i}KB\sin\phi[x_{jl} - lz_{jl}] &= H_{jl}, \\ c = 0, \quad j = 1, 2, 3, \ldots, \quad l = 1, \ldots, j. & \end{aligned} \right\} \tag{4.10b}$$

4.3. *The Stokes drift*

Upon collecting the zeroth harmonic terms from the continuity equation at order $O(\epsilon^j)$, and from the vorticity equation at order $O(\epsilon^{j+2})$, we obtain respectively two governing equations for x_{j0} and z_{j0}:

$$-KB\sin\phi\,\frac{\partial x_{j0}}{\partial c} + (1 - KB\cos\phi)\frac{\partial z_{j0}}{\partial c} = F_{j0}, \quad j = 1, 2, 3, \tag{4.11a}$$

$$(1 - KB\cos\phi)\frac{\partial^3 x_{j0}}{\partial c\,\partial t_1^2} + KB\sin\phi\,\frac{\partial^3 z_{j0}}{\partial c\,\partial t_1^2} - \Omega^2 KB\left[\cos\phi\,\frac{\partial x_{j0}}{\partial c} - \sin\phi\,\frac{\partial z_{j0}}{\partial c}\right] = G_{j0}, \quad j = 1, 2, 3. \tag{4.11b}$$

The dynamic free-surface boundary condition at $O(\epsilon^{j+1})$ yields

$$-KB\sin\phi\,\frac{\partial x_{j0}}{\partial a_1} + (1 - KB\cos\phi)\frac{\partial z_{j0}}{\partial a_1} = H_{j0}, \quad c = 0, \quad j = 1, 2, 3. \tag{4.11c}$$

In particular, (x_{10}, z_{10}) corresponds to the Stokes drift at the leading order. The forcing terms in (4.11 a–c) are

$$F_{10} = 0, \quad G_{10} = \frac{\partial}{\partial t_1}[2\sigma k\kappa_{\mathrm{r}}|A|^2\,\mathrm{e}^{2\kappa_{\mathrm{r}}c}], \quad H_{10} = 0. \tag{4.12a–c}$$

Performing t_1-integration of the vorticity equation $(4.11b)$–$(4.12b)$ and assuming zero vorticity at $t_1 = 0$, we deduce

$$(1 - KB\cos\phi)\frac{\partial^2 x_{10}}{\partial c\,\partial t_1} + KB\sin\phi\,\frac{\partial^2 z_{10}}{\partial c\,\partial t_1} - \Omega KB\left[\sin\phi\,\frac{\partial x_{10}}{\partial c} + \cos\phi\,\frac{\partial z_{10}}{\partial c}\right] = 2\sigma k\kappa_r|A|^2\,\mathrm{e}^{2\kappa_r c}.$$

$$(4.13)$$

It follows from the continuity equation $(4.11a)$ and $(4.12a)$ that

$$\frac{\partial z_{10}}{\partial c} = \frac{KB\sin\phi}{1 - KB\cos\phi}\frac{\partial x_{10}}{\partial c}, \tag{4.14}$$

where the denominator never vanishes since $KB < 1$. If (4.14) is substituted in (4.13), we obtain, after simplifications,

$$\left(\frac{\partial}{\partial t_1} - \frac{\Omega KB\sin\phi}{1 - KB\cos\phi}\right)x_{10} = \frac{1 - KB\cos\phi}{1 - 2KB\cos\phi + K^2 B^2}\sigma k|A|^2\,\mathrm{e}^{2\kappa_r c}, \tag{4.15}$$

which can be easily solved to give

$$\begin{pmatrix} x_{10} \\ z_{10} \end{pmatrix} = \left\{\sigma k\int_0^{t_1}\frac{|A|^2\,\mathrm{e}^{2\kappa_r c}}{1 - 2KB\cos\phi + K^2 B^2}\,\mathrm{d}t_1\right\}\begin{pmatrix} 1 - KB\cos\phi \\ KB\sin\phi \end{pmatrix}, \tag{4.16}$$

which satisfies the dynamic free-surface boundary condition $(4.11c)$–$(4.12c)$. If the long wave is absent, $KB = 0$, this Stokes drift takes the familiar form:

$$x_{10} = \sigma k\,\mathrm{e}^{2kc}\int_0^{t_1}|A|^2\,\mathrm{d}t_1, \quad z_{10} = 0. \tag{4.17}$$

Note that (4.16) is valid up to $(\Omega t_1, \phi) = O(1)$ which is sufficient for later purposes, but becomes unbounded as $\phi \sim \infty$. To get a uniformly valid solution for the Stokes drift itself one needs to add (x_0, z_0) in the series expansions (2.9).

The first-order short-wave displacement is now entirely determined:

$$\begin{pmatrix} x_1 \\ z_1 \end{pmatrix} = \left\{\sigma k\int_0^{t_1}\frac{|A|^2\,\mathrm{e}^{2\kappa_r c}}{1 - 2KB\cos\phi + K^2 B^2}\,\mathrm{d}t_1\right\}\begin{pmatrix} 1 - KB\cos\phi \\ KB\sin\phi \end{pmatrix} + \frac{1}{2}\begin{pmatrix} \mathrm{i} \\ 1 \end{pmatrix}A\mathrm{e}^{\mathrm{i}\tilde{S}}\,\mathrm{e}^{\kappa_r c} + \mathrm{c.c.},$$

$$(4.18)$$

where κ_r and κ_i are given by $(4.6a, b)$ and $\tilde{S}$ by (4.7).

4.4. *Linear evolution equation for the short wave*

Two governing equations for the first harmonic displacement at $O(\epsilon^2)$ are obtained from $(4.10a)$ with $(j, l) = (2, 1)$ and the forcing terms

$$F_{21} = \mathrm{i}\left\{k\left(\frac{\partial x_{10}}{\partial c} - \mathrm{i}\frac{\partial z_{10}}{\partial c}\right)A - (1 + KB\cos\phi + \mathrm{i}KB\sin\phi)\frac{\partial A}{\partial a_1}\right\}\mathrm{e}^{\kappa c}, \tag{4.19a}$$

$$G_{21} = \mathrm{i}\left\{k\left(\frac{\partial x_{10}}{\partial c} - \mathrm{i}\frac{\partial z_{10}}{\partial c}\right)A - (1 + KB\cos\phi + \mathrm{i}KB\sin\phi)\frac{\partial A}{\partial a_1}\right.$$

$$\left. - \frac{2}{\sigma}(1 - KB\cos\phi - \mathrm{i}KB\sin\phi)\frac{\partial\kappa}{\partial t_1}A\right\}\mathrm{e}^{\kappa c}. \tag{4.19b}$$

The free-surface boundary condition $(4.10b)$ for $(j, l) = (2, 1)$ is

$$(1 - KB\cos\phi + \mathrm{i}KB\sin\phi)(x_{21} - z_{21}) = H_{21}, \quad c = 0, \tag{4.20a}$$

with
$$H_{21} = -\frac{2i}{\sigma}(1 - KB\cos\phi - iKB\sin\phi)\left\{\frac{\partial A}{\partial t_1} + \frac{\sigma}{2k}\frac{\partial A}{\partial a_1}\right\}. \tag{4.20b}$$

The solution of the inhomogeneous matrix differential equation is

$$U = \frac{\frac{1}{2}}{1 - KB\cos\phi - iKB\sin\phi}\int^c [G_{21} + F_{21}]e^{-\kappa_r c' - i\kappa_i c'}\,dc'\begin{pmatrix}1\\1\end{pmatrix}e^{\kappa_r c + i\kappa_i c}$$

$$+ \frac{\frac{1}{2}}{1 - KB\cos\phi + iKB\sin\phi}\int_{-\infty}^c [G_{21} - F_{21}]e^{\kappa_r c' - i\kappa_i c'}\,dc'\begin{pmatrix}1\\-1\end{pmatrix}e^{-\kappa_r c + i\kappa_i c}, \tag{4.21}$$

where the lower limit of the first integral is left to be found. To evaluate the left-hand side of the dynamic condition on the free surface (4.20a), we note that the first integral in (4.21) does not contribute; the second term, however, gives

$$\{x_{21} - z_{21}\}_{c=0} = \frac{1}{1 - KB\cos\phi + iKB\sin\phi}\int_{-\infty}^0 [G_{21} - F_{21}]e^{\kappa_r c - i\kappa_i c}\,dc. \tag{4.22}$$

Comparison of (4.22) and (4.20a) then yields the solvability condition:

$$\int_{-\infty}^0 [G_{21} - F_{21}]e^{\kappa_r c - i\kappa_i c}\,dc = H_{21}. \tag{4.23}$$

Note from (4.19a, b) that (4.23) is independent of the Stokes drift. A similar condition holds for the first harmonic displacements at arbitrary order ϵ^j. After evaluating the integrand from (4.19a, b),

$$G_{21} - F_{21} = -\frac{2i}{\sigma}(1 - KB\cos\phi - iKB\sin\phi)\frac{\partial\kappa}{\partial t_1}A\,e^{\kappa_r c}e^{i\kappa_i c}, \tag{4.24}$$

it follows that
$$\frac{\partial A}{\partial t_1} + \frac{\sigma}{2k}\frac{\partial A}{\partial a_1} - \frac{1}{2\kappa_r}\frac{\partial\kappa}{\partial t_1}A = 0 \tag{4.25}$$

or, equivalently,

$$\frac{\partial A}{\partial t_1} + \frac{\sigma}{2k}\frac{\partial A}{\partial a_1} + \frac{\Omega KB\sin\phi}{1 - 2KB\cos\phi + K^2B^2}A - i\frac{\Omega KB}{1 - K^2B^2}\frac{(1 + K^2B^2)\cos\phi - 2KB}{1 - 2KB\cos\phi + K^2B^2}A = 0 \tag{4.26}$$

after using (4.6a, b). This equation governs the linear evolution of A over the scale range $(a_1, t_1) = O(1)$. Its implication for the short-wave modulation will be examined in §5.

With this solvability condition x_{21} and z_{21} can be completely determined:

$$\begin{pmatrix}x_{21}\\z_{21}\end{pmatrix} = \left\{i\sigma k^2\int_0^{t_1}\frac{|A|^2 e^{2\kappa_r c}\,dt_1}{1 - 2KB\cos\phi + K^2B^2} - ic\frac{1 + KB\cos\phi + iKB\sin\phi}{1 - KB\cos\phi - iKB\sin\phi}\frac{\partial A}{\partial a_1}\right.$$

$$\left. - \frac{2kc\Omega KB(KB - \cos\phi - i\sin\phi)}{(1 - KB\cos\phi - iKB\sin\phi)(1 - 2KB\cos\phi + K^2B^2)}A\right\}\begin{pmatrix}1\\1\end{pmatrix}e^{\kappa_r c}e^{i\kappa_i c}$$

$$- \frac{\Omega KB(\cos\phi + i\sin\phi)}{\sigma(1 - K^2B^2)}A\begin{pmatrix}1\\-1\end{pmatrix}e^{\kappa_r c}e^{i\kappa_i c}. \tag{4.27}$$

It is easy to show that the second harmonic vanishes, i.e. $(x_{22}, z_{22}) = (0, 0)$, since the corresponding forcing terms all vanish, $F_{22} = G_{22} = H_{22} = 0$.

4.5. *Nonlinear evolution equation for the short-wave amplitude*

We now invoke the solvability condition for (x_{31}, z_{31}):

$$\int_{-\infty}^{0} [G_{31} - F_{31}]\, e^{\kappa_r c - i\kappa_1 c}\, dc = H_{31}. \qquad (4.28)$$

From the lengthy expressions for G_{31} and F_{31}, we find, with the help of MACSYMA,

$$G_{31} - F_{31} = i(1 + KB\cos\phi - iKB\sin\phi)\left\{\frac{\partial x_{21}}{\partial a_1} - \frac{\partial z_{21}}{\partial a_1}\right\} - \frac{2kKB\sin\phi}{\sigma}\frac{\partial x_{21}}{\partial t_1}$$

$$- \frac{2i}{\sigma}(1 - KB\cos\phi)\frac{\partial^2 x_{21}}{\partial c\,\partial t_1} - \frac{2KB\sin\phi}{\sigma}\frac{\partial^2 z_{21}}{\partial c\,\partial t_1} + \frac{2ik}{\sigma}(1 + KB\cos\phi)\frac{\partial z_{21}}{\partial t_1}$$

$$+ ik(x_{21} - z_{21})\left\{\frac{\partial x_{10}}{\partial c} + i\frac{\partial z_{10}}{\partial c}\right\} - \frac{2k}{\sigma}\left(\frac{\partial A}{\partial t_1} + cA\frac{\partial \kappa}{\partial t_1}\right)\left(\frac{\partial x_{10}}{\partial c} - i\frac{\partial z_{10}}{\partial c}\right)e^{\kappa_r c}\,e^{i\kappa_1 c}$$

$$+ \left\{\frac{2c}{\sigma}(1 + KB\cos\phi + iKB\sin\phi)\frac{\partial \kappa}{\partial t_1}\frac{\partial A}{\partial a_1} + \frac{2}{\sigma}(1 + KB\cos\phi + iKB\sin\phi)\frac{\partial^2 A}{\partial a_1 \partial t_1}\right.$$

$$+ \frac{1}{\sigma^2}(1 - KB\cos\phi - iKB\sin\phi)\left(\frac{\partial^2 \kappa}{\partial t_1^2}A + 2c\left(\frac{\partial \kappa}{\partial t_1}\right)^2 A + 2\frac{\partial \kappa}{\partial t_1}\frac{\partial A}{\partial t_1}\right)$$

$$\left. - \frac{2k\Omega^2 KB(\cos\phi + i\sin\phi)}{\sigma^2(1 - KB\cos\phi - iKB\sin\phi)}A\right\}e^{\kappa_r c}\,e^{i\kappa_1 c}. \qquad (4.29)$$

The right-hand side of (4.28) is given by

$$H_{31} = -\frac{2i}{\sigma}(1 - KB\cos\phi)\frac{\partial x_{21}}{\partial t_1} - \frac{2KB\sin\phi}{\sigma}\frac{\partial z_{21}}{\partial t_1}$$

$$- \frac{KB\sin\phi}{k}\frac{\partial x_{21}}{\partial a_1} - \frac{i}{k}(1 - KB\cos\phi)\frac{\partial z_{21}}{\partial a_1} - A\left(\frac{\partial x_{10}}{\partial a_1} - i\frac{\partial z_{10}}{\partial a_1}\right)$$

$$- \frac{2i}{\sigma}(1 - KB\cos\phi - iKB\sin\phi)\left(\frac{\partial A}{\partial t_2} + \frac{\sigma}{2k}\frac{\partial A}{\partial x_2} + \frac{i}{2\sigma}\frac{\partial^2 A}{\partial t_1^2}\right), \quad c = 0. \qquad (4.30)$$

The solution (4.16) for x_{10} and z_{10}, (4.27) for x_{21} and z_{21} are now substituted in (4.29) and (4.30). After performing the integration, the result is found to be

$$\frac{\partial A}{\partial t_2} + \frac{\sigma}{2k}\frac{\partial A}{\partial a_2} + \frac{i\sigma}{8k^2}\frac{\partial^2 A}{\partial a_1^2} + \frac{i\sigma k^2 |A|^2 A}{2(1 - 2KB\cos\phi + K^2B^2)}$$

$$+ \frac{\Omega^2}{2\sigma}\frac{KB\sin\phi(1 + 2KB\cos\phi - 3K^2B^2)}{(1 - 2KB\cos\phi + K^2B^2)^2}A$$

$$+ \frac{i\Omega^2 KB}{2\sigma(1 - K^2B^2)^2}\frac{P_2(KB)\cos^2\phi + P_1(KB)\cos\phi + P_0(KB)}{(1 - 2KB\cos\phi + K^2B^2)^2}A = 0, \qquad (4.31)$$

where $P_j(KB)$ are the following polynomials:

$$P_2(KB) \equiv 2(KB)^5 + 4(KB)^3 - 2KB, \qquad (4.32a)$$

$$P_1(KB) \equiv -3(KB)^6 - 7(KB)^4 + 3(KB)^2 - 1 \qquad (4.32b)$$

and
$$P_0(KB) \equiv 7(KB)^5 - 6(KB)^3 + 3KB. \tag{4.32c}$$

Equation (4.31) governs the second-order evolution of A over $(a_2, t_2) = O(1)$. If ϵ times (4.31) is added to the linear evolution equation (4.26), a combined evolution equations valid for $(a_1, t_1) \leqslant O(1/\epsilon)$ is obtained:

$$\frac{\partial A}{\partial t_1} + \frac{\sigma}{2k}\frac{\partial A}{\partial a_1} + \frac{\Omega KB \sin \phi}{1 - 2KB \cos \phi + K^2 B^2} A - i \frac{\Omega KB}{1 - K^2 B^2} \frac{(1 + K^2 B^2)\cos \phi - 2KB}{1 - 2KB \cos \phi + K^2 B^2} A$$

$$+ \frac{i\epsilon\sigma}{8k^2}\frac{\partial^2 A}{\partial a_1^2} + \frac{i\epsilon\sigma K^2 |A|^2 A}{2(1 - 2KB \cos \phi + K^2 B^2)} + \frac{\epsilon\Omega^2}{2\sigma}\frac{KB \sin \phi (1 + 2KB \cos \phi - 3K^2 B^2)}{(1 - 2KB \cos \phi + K^2 B^2)^2} A$$

$$+ \frac{i\epsilon\Omega^2 KB}{2\sigma(1 - K^2 B^2)^2} \frac{P_2(KB)\cos^2\phi + P_1(KB)\cos\phi + P_0(KB)}{(1 - 2KB \cos \phi + K^2 B^2)^2} A = O(\epsilon^2). \tag{4.33}$$

This is a cubic nonlinear Schrödinger equation with periodiuc coefficients expressed explicitly in terms of the long Gerstner wave. It reduces to the familiar equation in the limit of $KB = 0$.

By the following change of variables:

$$\xi' = a_1 - \frac{\sigma}{2k}t_1, \quad \phi = \Omega t_1 - \epsilon K a_1, \tag{4.34a, b}$$

it can be shown that

$$\frac{\partial A}{\partial \phi} = -\frac{1}{\delta}\frac{KB \sin \phi}{1 - 2KB \cos \phi + K^2 B^2} A + \frac{iKB}{\delta(1 - K^2 B^2)}\frac{(1 + K^2 B^2)\cos \phi - 2KB}{1 - 2KB \cos \phi + K^2 B^2} A$$

$$- \frac{i\epsilon\sigma}{8\delta\Omega k^2}\frac{\partial^2 A}{\partial \xi'^2} - i\frac{\epsilon\sigma k^2}{2\delta\Omega}\frac{|A|^2 A}{(1 - 2KB \cos \phi + K^2 B^2)} - \frac{\epsilon\Omega}{2\delta\sigma}\frac{KB \sin \phi (1 + 2KB \cos \phi - 3K^2 B^2)}{(1 - 2KB \cos \phi + K^2 B^2)^2} A$$

$$- \frac{i\epsilon\Omega KB}{2\delta\sigma(1 - K^2 B^2)^2}\frac{P_2(KB)\cos^2\phi + P_1(KB)\cos\phi + P_0(KB)}{(1 - 2KB \cos \phi + K^2 B^2)^2} A = O(\epsilon^2), \tag{4.35}$$

where
$$\delta \equiv 1 - \epsilon(\Omega/2\sigma). \tag{4.36}$$

The ϕ-dependent coefficients in (4.35) are 2π-periodic. For further simplification, we introduce the following transformation to remove the linear and imaginary term on the right:

$$A(\xi, \phi) = \bar{A}\mathscr{A}(\xi', \phi)e^{i\Gamma}, \quad \xi = \xi' k^2 \bar{A}, \tag{4.37}$$

where $\bar{A}$ is the short-wave amplitude in the absence of the long wave. It then follows that

$$\Gamma(\phi; KB, \epsilon) = \frac{1}{\delta}\left[\arctan\left\{\frac{1 + KB}{1 - KB}\frac{\sin \phi}{1 + \cos \phi}\right\} - \frac{1 + K^2 B^2}{1 - K^2 B^2}\arctan\left\{\frac{\sin \phi}{1 + \cos \phi}\right\}\right]$$

$$+ \frac{\epsilon\Omega}{2\sigma\delta}\left[\frac{2KB \sin \phi}{1 - 2KB \cos \phi + K^2 B^2} - \arctan\left\{\frac{1 + KB}{1 - KB}\frac{\sin \phi}{1 + \cos \phi}\right\}\right.$$

$$\left. - \frac{B^4 K^4 + 2B^2 K^2 - 1}{(1 - B^2 K^2)^2}\arctan\left\{\frac{\sin \phi}{1 + \cos \phi}\right\}\right] \tag{4.38}$$

and

$$\frac{\partial \mathscr{A}}{\partial \phi} = -\frac{1}{\delta} \frac{KB \sin \phi}{1 - 2KB \cos \phi + K^2 B^2} \left[1 + \frac{\epsilon}{2} \frac{\Omega}{\sigma} \frac{1 + 2KB \cos \phi - 3K^2 B^2}{1 - 2KB \cos \phi + K^2 B^2} \right] \mathscr{A}$$
$$-\frac{i\alpha}{4} \frac{\partial^2 \mathscr{A}}{\partial \xi^2} - \frac{i\alpha |\mathscr{A}|^2 \mathscr{A}}{1 - 2KB \cos \phi + K^2 B^2} + O(\epsilon^2), \quad (4.39)$$

where the parameter α is defined by

$$\alpha = \frac{\epsilon}{2\delta} \frac{\sigma}{\Omega} (k\bar{A})^2. \qquad (4.40)$$

5. Linear modulation of short waves

5.1. *Amplitude modulation*

Over the timescale of a long-wave period, the short-wave modulation is governed by the linear equation (4.25), i.e. the $O(1)$ terms of (4.33). Now the moving frame is sufficiently well described by

$$\xi = a_1 - \frac{\sigma}{2k} t_1, \quad \phi = \Omega t_1. \qquad (5.1\,a, b)$$

The magnitude $|A|$ of the short-wave amplitude satisfies

$$\frac{\partial |A|}{\partial \phi} = \frac{-KB \sin \phi}{1 - 2KB \cos \phi + K^2 B^2} |A|, \qquad (5.2)$$

which can be integrated to give

$$\frac{|A|}{\bar{A}} = (1 - 2KB \cos \phi + K^2 B^2)^{-\frac{1}{2}}, \qquad (5.3)$$

where $\bar{A}$ refers to the amplitude without the long wave. (Note that $\bar{A}$ is also the amplitude at the zero-crossing, cf. (3.8)). When the long-wave slope is small, $KB \ll 1$, the well-known result of Longuet-Higgins & Stewart (1960) is recovered:

$$\frac{|A|}{\bar{A}} = 1 + KB \cos \phi + O(K^2 B^2). \qquad (5.4)$$

For finite KB, the normalized short-wave amplitude at the crest ($\phi = 0$), the trough ($\phi = \pi$) and at the point where the free surface of the long wave crosses the calm sea surface ($\cos \phi = -\frac{1}{2} KB$) are given by

$$\frac{|A|_{\text{crest}}}{\bar{A}} = \frac{1}{1 - KB}, \quad \frac{|A|_{\text{trough}}}{\bar{A}} = \frac{1}{1 + KB}, \qquad (5.5\,a, b)$$

$$\frac{|A|_{\text{crossing}}}{\bar{A}} = \frac{1}{(1 + 2K^2 B^2)^{\frac{1}{2}}}. \qquad (5.5\,c)$$

Equation (5.2) may also be written as

$$\frac{\partial}{\partial \phi} (g_{\text{eff}} |A|) = 0, \qquad (5.6)$$

where $$g_{\mathrm{eff}}/g = (1 + K^2 B^2 - 2KB \cos \phi)^{\frac{1}{2}} \qquad (5.7)$$

is the effective gravity experienced by the short wave due to the acceleration g' of the long-wave surface, i.e.

$$\boldsymbol{g}_{\mathrm{eff}} = \boldsymbol{g} - \boldsymbol{g}', \qquad (5.8)$$

with $$\boldsymbol{g}' = \left(\frac{\partial^2 X_2}{\partial t_1^2}, \frac{\partial^2 Z_2}{\partial t_1^2} \right)_{c_2 = 0} = -gKB \, (\sin \phi, \cos \phi). \qquad (5.9)$$

The variation of g_{eff}/g *vs.* ϕ is compared with the calculations of Longuet-Higgins (1987) in figure 2 below; the agreement is rather good.

Alternatively, (5.6) may be expressed as

$$\frac{\partial}{\partial t_1} (g_{\mathrm{eff}}^2 |A|^2) + \frac{\partial}{\partial a_1} (C_{\mathrm{g}} \, g_{\mathrm{eff}}^2 |A|^2) = 0, \qquad (5.10)$$

which plays the same role as the law of wave-action conservation (Bretherton & Garrett 1969; Henyey *et al.* 1988).

5.2. *Wavenumber modulation*

In view of (4.26) the short-wave phase $\tilde{S}$ must be corrected to incorporate the effect of the phase $\varGamma$ of A, i.e.

$$S = \tilde{S} + \varGamma(\phi, KB, 0) + O(\epsilon) = k \left[a + \frac{2KB \sin \phi}{1 - 2KB \cos \phi + K^2 B^2} c \right] - \omega t + \varGamma(\phi, KB, 0) + O(\epsilon).$$
$$(5.11)$$

Let us pass from the Lagrangian to the Eulerian reference frame by the transformation

$$a = X - \frac{B}{\epsilon^2} \sin \phi \, \mathrm{e}^{Kc_2} + O(\epsilon), \quad c = Z - \frac{B}{\epsilon^2} \cos \phi \, \mathrm{e}^{Kc_2} + O(\epsilon), \qquad (5.12)$$

Upon substituting (5.12) into (5.11), we obtain

$$S = \frac{1}{\epsilon^2} S_{-2} + S_0 + O(\epsilon), \qquad (5.13a)$$

where $$S_{-2} = -\frac{k(1 + K^2 B^2) B \sin \phi}{1 - 2KB \cos \phi + K^2 B^2} \mathrm{e}^{Kc_2} \qquad (5.13b)$$

and $$S_0 = k \left[X + \frac{2KB \sin \phi}{1 - 2KB \cos \phi + K^2 B^2} Z \right] - \sigma t + \varGamma(\phi, KB, 0). \qquad (5.13c)$$

Note that S_2 and $\varGamma$ depend on X_2 and Z_2 through ϕ and c_2, and on t_1, whereas S_0 depends on the fast Eulerian scales (X, Z, t). In the Eulerian frame, the wavenumber vector $\boldsymbol{k}^{\mathrm{E}}$ should be the Eulerian spatial gradient of the phase, i.e.

$$\boldsymbol{k}^{\mathrm{E}} = \nabla S + \epsilon \nabla_1 S + \epsilon^2 \nabla_2 S + O(\epsilon) = \nabla S_0 + \nabla_2 S_{-2} + O(\epsilon), \qquad (5.14)$$

where ∇ and ∇_i stand respectively for (∂_X, ∂_Z) and $(\partial_{X_i}, \partial_{Z_i})$. Since $\varGamma$ is independent of the fast coordinate X, it does not contribute to the wavenumber at the leading

order. S_{-2} is a function of both ϕ and c_2 and we obtain, in accordance with the chain rule,

$$\mathbf{k}^{\mathrm{E}} = \nabla S_0 + \frac{\partial S_{-2}}{\partial a_2}\nabla_2 a_2 + \frac{\partial S_{-2}}{\partial c_2}\nabla_2 c_2, \tag{5.15}$$

i.e.

$$\mathbf{k}^{\mathrm{E}} = \nabla S_0 + K\left[S_{-2}\nabla_2 c_2 - \frac{\partial S_{-2}}{\partial \phi}\nabla_2 a_2\right]. \tag{5.16}$$

The horizontal component of $\mathbf{k}^{\mathrm{E}}$ is then

$$k_x^{\mathrm{E}} = \frac{\partial S_0}{\partial X} - \frac{K}{1-K^2B^2}\left[KB\cos\phi S_{-2} + (1+KB\cos\phi)\frac{\partial S_{-2}}{\partial \phi}\right] + O(\epsilon), \tag{5.17}$$

i.e.

$$\frac{k_x^{\mathrm{E}}}{k} = \frac{1-3KB\cos\phi+4K^2B^2\cos^2\phi-2K^3B^3\cos\phi\sin^2\phi}{(1-K^2B^2)(1-2KB\cos\phi+K^2B^2)^2}$$

$$+ \frac{-K^4B^4(1+4\cos^2\phi)+K^5B^5\cos\phi(1+2\cos^2\phi)}{(1-K^2B^2)(1-2KB\cos\phi+K^2B^2)^2} + O(\epsilon). \tag{5.18}$$

For small KB, (5.18) reduces to the classical result of Longuet-Higgins & Stewart (1960):

$$\frac{k_x^{\mathrm{E}}}{k} = 1 + KB\cos\phi + O(\epsilon). \tag{5.19}$$

For finite KB, k_x^{E} has the following values at the long-wave crest, trough, and the point of zero-crossing:

$$\frac{k_{x\,\mathrm{crest}}^{\mathrm{E}}}{k} = \frac{1-2KB+3K^2B^2}{(1-KB)^3}, \quad \frac{k_{x\,\mathrm{trough}}^{\mathrm{E}}}{k} = \frac{1+2KB+3K^2B^2}{(1+KB)^3}, \tag{5.20a,b}$$

and

$$\frac{k_{x\,\mathrm{crossing}}^{\mathrm{E}}}{k} = \frac{1+\frac{3}{2}K^2B^2+K^4B^4-\frac{7}{4}K^6B^6-\frac{1}{4}K^8B^8}{(1-K^2B^2)(1+2K^2B^2)^2}. \tag{5.20c}$$

Note that k_x^{E} is positive at the crest, the trough, and at the zero-crossing of the long wave.

Next, the vertical component of the wavenumber k_z^{E} is, to leading order,

$$k_z^{\mathrm{E}} = \frac{\partial S_0}{\partial Z} + \frac{K}{1-K^2B^2}\left[(1-KB\cos\phi)S_{-2} + KB\sin\phi\frac{\partial S_{-2}}{\partial \phi}\right] + O(\epsilon), \tag{5.21}$$

so that

$$\frac{k_z^{\mathrm{E}}}{k} = \frac{KB\sin\phi}{(1-K^2B^2)(1-2KB\cos\phi+K^2B^2)^2}$$

$$\times [1-2KB\cos\phi-2K^2B^2\cos^2\phi+6K^3B^3\cos\phi-K^4B^4(1+2\cos^2\phi)]+O(\epsilon). \tag{5.22}$$

Note in particular that

$$\frac{k_{z\,\mathrm{crest}}^{\mathrm{E}}}{k} = \frac{k_{z\,\mathrm{trough}}^{\mathrm{E}}}{K} = 0, \tag{5.23a,b}$$

$$\frac{k_{z\,\mathrm{crossing}}^{\mathrm{E}}}{k} = \frac{\pm KB(1+K^2B^2-\frac{9}{2}K^4B^4-\frac{1}{2}K^6B^6)(1-\frac{1}{4}K^2B^2)^{\frac{1}{2}}}{(1-K^2B^2)(1+2K^2B^2)^2}. \tag{5.23c}$$

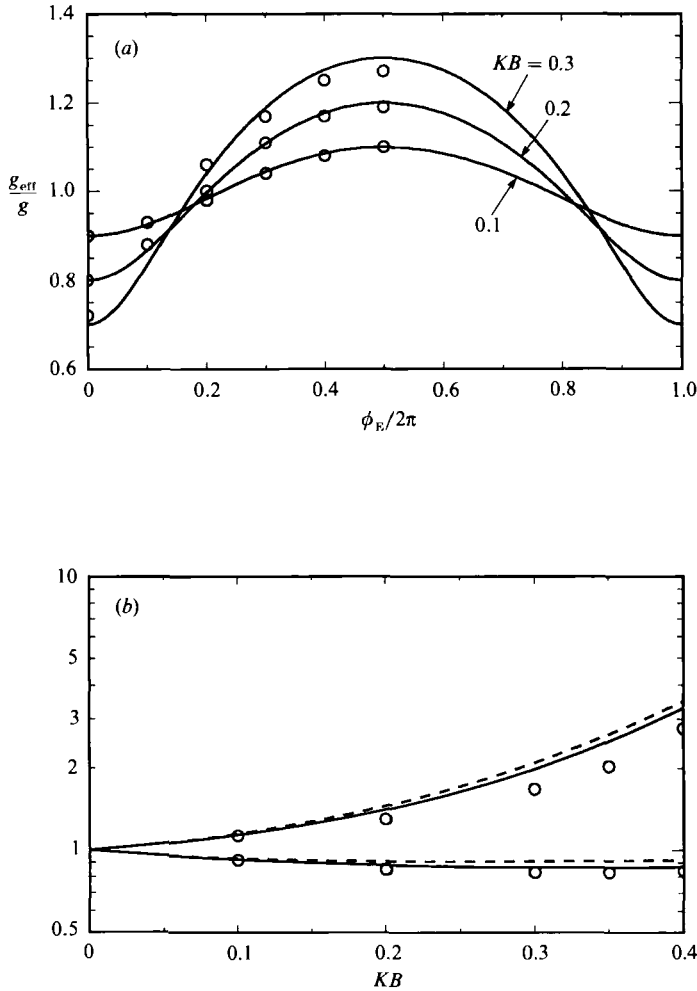FIGURE 2(a, b). For caption see facing page.

For small KB, we have

$$\frac{k_{z\,\mathrm{crossing}}}{k} = \pm KB + O(K^3 B^3). \tag{5.24}$$

Combining (5.18) and (5.22) we get

$$\frac{k^{\mathrm{E}}}{k} = [1 - 6KB \cos\phi + K^2 B^2 (1 + 16\cos^2\phi) - 8K^3 B^3 \cos\phi(1 + 2\cos^2\phi)$$

$$+ 2K^4 B^4(-1 + 2\cos^2\phi + 2\cos^4\phi) + 4K^5 B^5 \cos\phi(5 + 2\cos^2\phi + 2\cos^4\phi)$$

$$- 2K^6 B^6(1 + 18\cos^2\phi + 10\cos^4\phi)$$

$$+ 8K^7 B^7 \cos\phi(1 + 2\cos^4\phi) + K^8 B^8(1 + 44\cos^2\phi - 20\cos^4\phi)$$

$$- 2K^9 B^9 \cos\phi(7 + 12\cos^2\phi - 4\cos^4\phi)$$

$$+ K^{10} B^{10}(1 + 4\cos^2\phi + 4\cos^4\phi)]^{\frac{1}{2}} \times (1 - K^2 B^2)^{-1}(1 - 2KB\cos\phi + K^2 B^2)^{-2}. \tag{5.25}$$

Its value at the zero-crossing can be easily obtained by setting $\cos\phi = -\frac{1}{2}KB$.
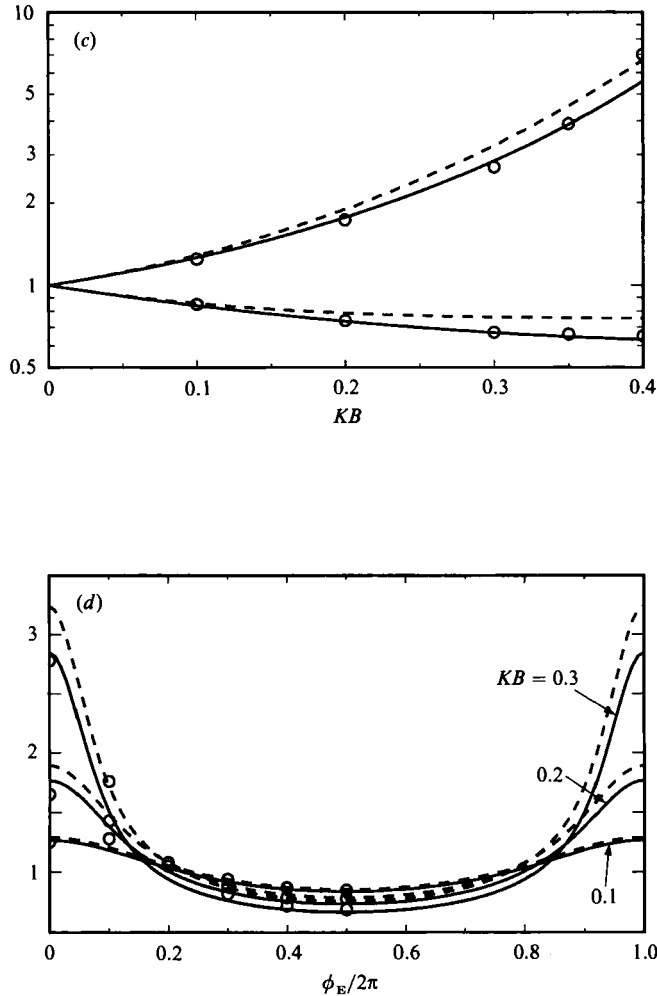
FIGURE 2. Comparison of present theory with Longuet-Higgins (1987, marked here by $\bigcirc$). (a) Variation of effective gravity along the phase of a long wave. (b) Normalized wavenumber of the short wave at the crest ($k_1 = k_{\text{crest}}/k_{\text{crossing}}$, upper curves) and the trough ($k_2 = k_{\text{trough}}/k_{\text{crossing}}$, lower curves) of the long wave. (c) Normalized short-wave steepness at the crest ($r_1 = (k^{\text{E}}A)_{\text{crest}}/(k^{\text{E}}A)_{\text{crossing}}$) and trough ($r_2 = (k^{\text{E}}A)_{\text{trough}}/(k^{\text{E}}A)_{\text{crossing}}$) of the long wave. (d) Normalized short-wave steepness ($r = k^{\text{E}}A/(k^{\text{E}}A)_{\text{crossing}}$) along the phase of a long wave. In (b–d) solid lines are based on zero-crossing of the Stokes wave, dashed lines on zero-crossing of the Gerstner wave.

We now compare these analytical formulae with the numerical results by Longuet-Higgins (1987) for irrotational long waves of finite steepness. First, he plotted k/k_{crossing} and $kA/(kA)_{\text{crossing}}$, where the subscript 'crossing' refers to zero crossing of the long Stokes wave. Among three sets of his calculations, for $k_{\text{crossing}}/K = 2, 10, 100$, we choose the last with the largest scale contrast for comparison. Since the zero-crossings of Stokes wave are different from those of Gerstner's wave by $O(KB)$, we plotted our results according to two normalizations, one by $\bar{k}$ at the Stokes-wave crossing, as solid lines, and one by $\bar{k}$ at the Gerstner-wave crossing, as dashed lines. For the range $0 < KB < 0.4$, the short wavenumbers at the long-wave crests and troughs are compared in figure 2(b), and the corresponding short-wave steepnesses in figure 2(c). Variation of the steepness ratio of the short wave over one

long wavelength is compared in figure $2(d)$ for $KB = 0.1, 0.2$ and 0.3. The agreement with Longuet-Higgins is somewhat better by the first normalization. Crudely speaking, the agreement is within $O(K^2B^2)$ for both normalizations, consistent with the difference in vorticity.

Finally, we compare the inclination of the short wave k^{E},

$$\tan \vartheta = k_z^{\mathrm{E}}/k_x^{\mathrm{E}}, \tag{5.26}$$

with the inclination of the long-wave surface

$$\tan \vartheta_{\mathrm{Gerst}} = \left(\frac{\partial Z_2}{\partial a_2} \bigg/ \frac{\partial X_2}{\partial a_2}\right)_{c_2 = 0} = \frac{KB \sin \phi}{1 - KB \cos \phi} \tag{5.27}$$

after using (II.5.9.a–c). Straightforward manipulations show that the difference between the two slopes is of $O(K^3B^3)$ for small KB. Therefore the short wave essentially propagates along the surface of the long wave.

5.3. *Dispersion relation in the Eulerian frame*

In existing theories where both long and short waves are assumed to be irrotational, it is known that the dispersion relation of the short wave can be written as

$$\sigma^2 = g_{\mathrm{eff}} k^{\mathrm{E}} \tag{5.28}$$

Here (4.9) can be rewritten in terms of the Eulerian short-wave wavenumber k^{E} and the effective gravity as follows

$$\sigma^2 = g_{\mathrm{eff}} k^{\mathrm{E}} \frac{g}{g_{\mathrm{eff}}} \frac{k}{k^{\mathrm{E}}}, \tag{5.29}$$

where g_{eff}/g is given by (5.7) and k^{E}/k by (5.25). For small KB, we have

$$\frac{g}{g_{\mathrm{eff}}} \frac{k}{k^{\mathrm{E}}} = 1 - 2K^2B^2 \cos^2 \phi + O(K^3B^3) \tag{5.30}$$

Thus (5.29) differs from (5.28) by the same order as the vorticity in Gerstner's long waves.

5.4. *Absolute and intrinsic frequencies*

We now examine the *absolute* frequency ω of the short waves, as seen by an observer fixed in space, which is to be distinguished from the *intrinsic* frequency σ seen by an oscillatory fluid particle,

$$\omega = -\frac{\partial S}{\partial t}\bigg|_{X, X_1} - \epsilon \frac{\partial S}{\partial t_1}\bigg|_{X, X_1} + O(\epsilon) = -\frac{1}{\epsilon}\frac{\partial S_{-2}}{\partial \phi}\frac{\partial \phi}{\partial t_1}\bigg|_{X, X_1} + \sigma + O(\epsilon), \tag{5.31}$$

where the time derivatives are taken by fixing the Eulerian coordinates. Again the contribution from Γ is negligible. Note from (3.6b) that

$$\frac{\partial \phi}{\partial t_1}\bigg|_{X, X_1} = \frac{\partial \phi_{\mathrm{E}}}{\partial t_1}\bigg|_{X, X_1}(1 - KB \cos \phi)^{-1} = \frac{\Omega}{1 - KB \cos \phi}. \tag{5.32}$$

With the help of the dispersion relations, the normalized absolute frequency is simply

$$\frac{\omega}{\sigma} = 1 + \frac{1}{\epsilon}\frac{\sigma}{\Omega}KB \frac{1 + K^2B^2}{1 - KB \cos \phi} \frac{-2KB + (1 + K^2B^2)\cos \phi}{(1 - 2KB \cos \phi + K^2B^2)^2} + O(\epsilon). \tag{5.33}$$
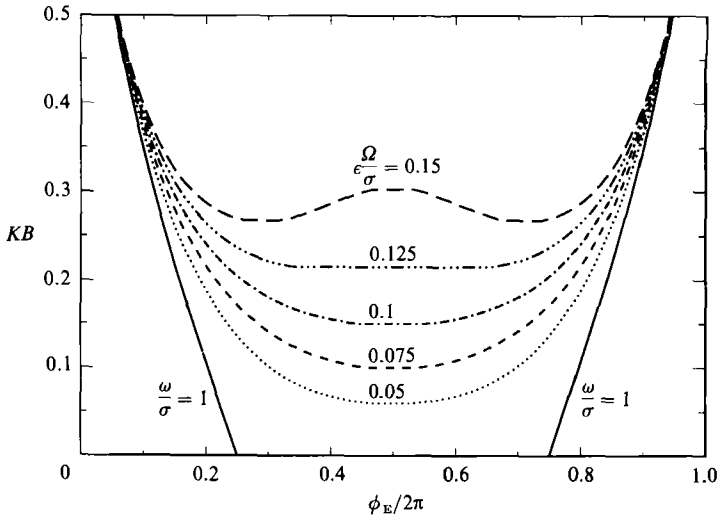
FIGURE 3. Contours of ω/σ in the $(KB, \phi_{\rm E})$-plane. Solid lines: $\omega/\sigma = 1$. Other lines correspond to $\omega/\sigma = 0$ for various $\epsilon\Omega/\sigma$.

Owing to the ratio $(1/\epsilon)\,(\sigma/\Omega)$, the difference between intrinsic and absolute frequencies can be large. Also, they can be equal to two points in a long-wave phase if

$$\cos\phi = \frac{2KB}{1 + K^2 B^2}. \qquad (5.34)$$

The Eulerian phase corresponding to the solution of (5.34) is shown by two solid curves in figure 3. Also shown are the curves along which the absolute frequency ω vanishes, for a range $\epsilon\Omega/\sigma$. If $KB < (KB)_{\rm min} \sim \epsilon\Omega/\sigma, \omega(\phi_{\rm E})$ is always positive for all $\phi_{\rm E}$, implying that the short waves propagate to the right everywhere for the length of a long wave. For $KB > (KB)_{\rm min}$, $\omega(\phi)$ may assume negative values in the neighbourhood of $\phi_{\rm E} = \pi$. To a fixed observer the short wave propagates to the left, hence appears to be reflected, in the trough of a long wave.

6. Linearized sideband instability of a short Stokes wave

As in the classical case without long waves (Benjamin & Feir 1967), we first examine the instability of a Stokes wave subject to sideband disturbances.

6.1. *Short Stokes wave on a long wave*

We define the short Stokes wave to be the solution of (4.39) independent of ξ, i.e.

$$\mathscr{A}_{\rm s}(\phi) = |\mathscr{A}_{\rm s}(\phi)|\,{\rm e}^{{\rm i}\beta(\phi)}, \qquad (6.1)$$

where both $|\mathscr{A}_{\rm s}|$ and β are real. It is an extension of the classical Stokes wave when the long wave is absent. Substitution of (6.1) in (4.19) yields

$$\frac{\partial|\mathscr{A}_{\rm s}|}{\partial\phi} = -Q\left(\phi, KB, \epsilon\frac{\Omega}{\sigma}\right)|\mathscr{A}_{\rm s}|, \quad \frac{\partial\beta}{\partial\phi} = -\frac{\alpha|\mathscr{A}_{\rm s}|^2}{1 - 2KB\cos\phi + K^2 B^2}, \qquad (6.2a, b)$$

where

$$Q\left(\phi, KB, \epsilon\frac{\Omega}{\sigma}\right) = \frac{1}{\delta}\frac{KB\sin\phi}{1 - 2KB\cos\phi + K^2 B^2}\left[1 + \frac{\epsilon}{2}\frac{\Omega}{\sigma}\frac{1 + 2KB\cos\phi - 3K^2 B^2}{1 - 2KB\cos\phi + K^2 B^2}\right] \qquad (6.2c)$$
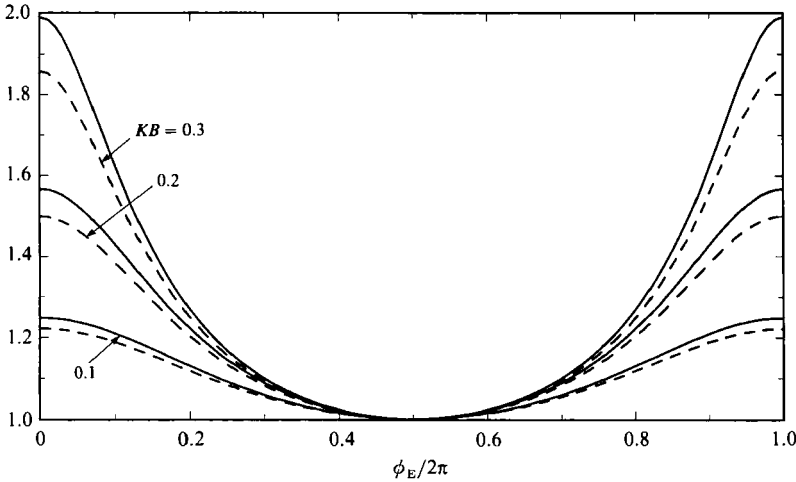
FIGURE 4. Amplitude variation of the short Stokes wave $|\mathscr{A}|_{\rm s}$ as a function of the long-wave phase. For comparison the linearized approximation given by $A/\bar{A}$ in (5.3) is shown by dashed curves.

and α is defined by (4.40). The solution is

$$|\mathscr{A}_{\rm s}(\phi)| = \left(\frac{N(\phi_0)}{N(\phi)}\right)^{\frac{1}{2}} \exp\left\{\frac{\epsilon}{2\delta}\frac{\Omega}{\sigma}(1-K^2B^2)\left(\frac{1}{N(\phi)}-\frac{1}{N(\phi_0)}\right)\right\}, \qquad (6.3a)$$

where

$$N(\phi) = 1 - 2KB\cos\phi + K^2B^2. \qquad (6.3b)$$

Note that the leading-order term in (6.3) is identical to (5.3) since $\phi = \Omega t_1 + O(\epsilon)$, while the correction due to the long wave is represented by the exponential term. Nonlinearity of the short wave does not affect this quantity, as in the Stokes wave in calm water. In figure 4 the variations of $|\mathscr{A}_{\rm s}|$ along with $|A|/\bar{A}$ (as defined by (5.3)) are plotted against the Eulerian phase $\phi_{\rm E}$ of the long wave for several KB. The phase β is then given by

$$\beta\left(\phi, \epsilon\frac{\Omega}{\omega}\right) = -\alpha \int_{\phi_0}^{\phi} G\left(\phi'; \frac{\epsilon\Omega}{\sigma}\right)\mathrm{d}\phi', \qquad (6.4a)$$

where

$$G\left(\phi, \epsilon\frac{\Omega}{\sigma}\right) = \frac{|\mathscr{A}_{\rm s}(\phi)|^2}{N(\phi)}. \qquad (6.4b)$$

The corresponding nonlinear modification of the Lagrangian wavenumber and frequency are defined by

$$\Delta k = \left(\frac{\partial}{\partial a}+\epsilon^2\frac{\partial}{\partial a_2}\right)\beta, \quad \Delta\sigma = -\left(\frac{\partial}{\partial t}+\epsilon\frac{\partial}{\partial t_1}\right)\beta. \qquad (6.5a,b)$$

It follows straightforwardly that

$$\Delta k = \epsilon^2\frac{\partial\phi}{\partial a_2}\frac{\partial\beta}{\partial\phi} = \alpha\epsilon^2 KG = O(\epsilon^3), \qquad (6.6)$$

which is negligible, and

$$\Delta\sigma = -\epsilon\frac{\partial\phi}{\partial t_1}\frac{\partial\beta}{\partial\phi} = \epsilon\alpha\Omega G + O(\epsilon^3) \qquad (6.7)$$

or
$$\frac{\Delta\sigma}{\sigma} = \epsilon\alpha\frac{\Omega}{\sigma}G = \tfrac{1}{2}\epsilon^2(k\bar{A})^2 G + O(\epsilon^3),\tag{6.8}$$

where use is made of the definition (4.40) of α. Again, for $KB = 0$, $G(\phi) = 1$ and the classical result is recovered:
$$\frac{\Delta\sigma}{\sigma} = \tfrac{1}{2}\epsilon^2(k\bar{A})^2 + O(\epsilon^3).\tag{6.9}$$

We remark that the solution by Zhang & Melville (1990) for a steady short wave, with both amplitude and phase locked to the irrotational long-wave profile, has a more complicated form than (6.3) here.

6.2. *Linear instability of the short Stokes wave*

Upon substituting
$$\mathscr{A}(\xi,\phi) = \mathscr{A}_s(\phi)\,\tilde{\mathscr{A}}(\xi,\phi)\tag{6.10}$$

into (4.39) we get the canonical form of the evolution equation,
$$\frac{\partial\tilde{\mathscr{A}}}{\partial\phi} = -\frac{i\alpha}{4}\frac{\partial^2\tilde{\mathscr{A}}}{\partial\xi^2} - i\alpha G\left(\phi;\frac{\epsilon\Omega}{\sigma}\right)|\tilde{\mathscr{A}}|^2\tilde{\mathscr{A}}.\tag{6.11}$$

Let the amplitude b and phase $\int^\xi W\,\mathrm{d}\xi$ of $\tilde{\mathscr{A}}$ be defined by
$$\tilde{\mathscr{A}} = b\exp\left(i\int^\xi W\,\mathrm{d}\xi\right),\tag{6.12}$$

where both $b(\xi,\phi)$ and $W(\xi,\phi)$ are real. Equation (6.11) can be split into two real equations:
$$\frac{\partial b}{\partial\phi} = \frac{\alpha}{4}\left[\frac{\partial(bW)}{\partial\xi} + W\frac{\partial b}{\partial\xi}\right]\tag{6.13a}$$

and
$$\frac{\partial W}{\partial\phi} = -\alpha\frac{\partial}{\partial\xi}\left\{\frac{1}{4}\left[\frac{1}{b}\frac{\partial^2 b}{\partial\xi^2} - W^2\right] + Gb^2\right\}.\tag{6.13b}$$

In view of (6.10), the Stokes wave corresponds to $b_0 = 1$ and $W_0 = 0$. We then consider wave-like perturbations:
$$b = 1 + \tilde{b}\mathrm{e}^{i\xi\nu},\quad W = \tilde{W}\mathrm{e}^{i\nu\xi}.\tag{6.14}$$

For infinitesimal $\tilde{b}, \tilde{W}$ the linearized equations are
$$\frac{\partial\tilde{b}}{\partial\phi} = i\frac{\alpha\nu}{4}\tilde{W}\tag{6.15a}$$

and
$$\frac{\partial\tilde{W}}{\partial\phi} = -2i\alpha\nu\left[G - \frac{\nu^2}{8}\right]\tilde{b}.\tag{6.15b}$$

Since $G(\phi;\epsilon\Omega/\sigma)$ is 2π-periodic in ϕ, Floquet theory is needed. By a standard numerical procedure (cf. Nayfeh & Mook 1979 and Iooss & Joseph 1980), we first compute the Floquet multipliers $\mu_{1,2}$ and then deduce the growth rates as $\ln|\mu_{1,2}|$.

For $\epsilon k\bar{A} = 0.13$, $\epsilon\Omega/\sigma = 0.07$, which corresponds to $\alpha = 0.125$, we display the effects of varying KB and the sideband wavenumber ν. Only the larger of the two growth rates $\ln|\mu_{1,2}|$ is plotted versus ν and KB, in figure 5. First, when the long wave is absent, the band of instability reduces to that of Benjamin & Feir with the
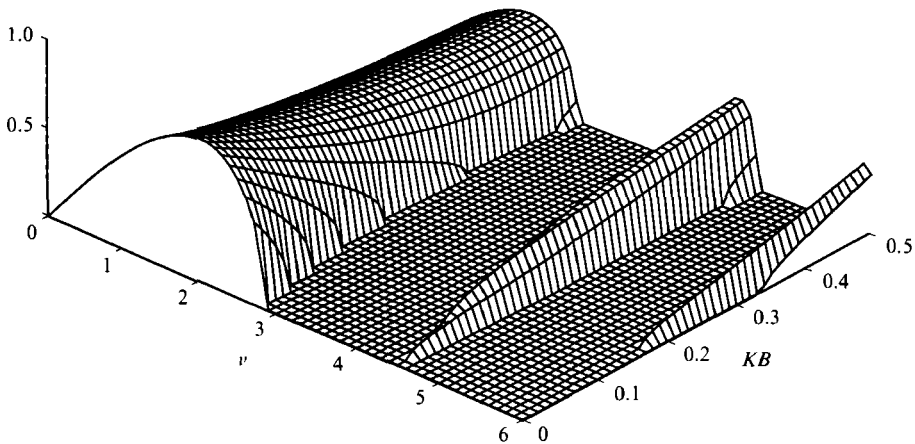
FIGURE 5. Linear growth rate as a function of long-wave slope KB and disturbance wavenumber ν, with $\epsilon k \bar{A} = 0.13$ and $\alpha = 0.125$.
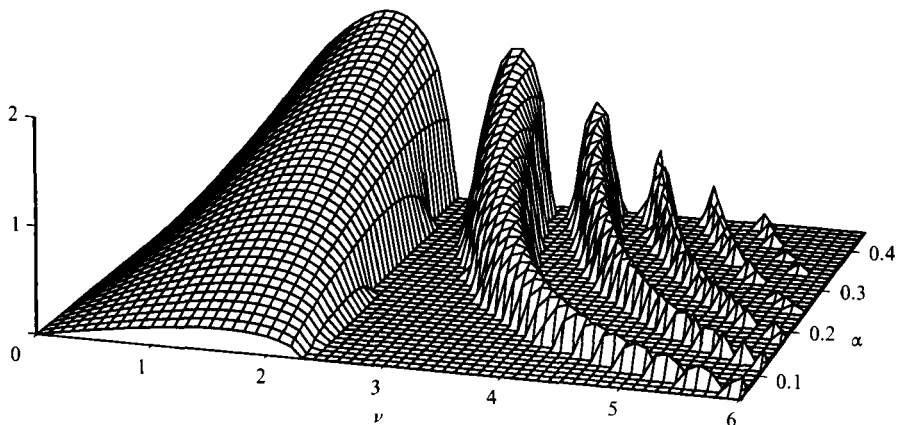

FIGURE 6. Linear growth rate as a function of short wave α and disturbance wavenumber ν, with $KB = 0.3$ and $\epsilon k \bar{A} = 0.13$.

bandwidth given by $0 \leqslant \nu \leqslant 2\sqrt{2}$. When the long-wave slope increases, the unstable bandwidth decreases slightly at first, then increases again. Furthermore, the maximum growth rate decreases and levels off as KB increases. For sufficiently large ν, new bands of instability emerge, and their maximum growth rate increases monotonically with KB.

The parameter α increases with increasing short-wave steepness $\epsilon k \bar{A}$ and with decreasing frequency ratio $\epsilon \Omega / \sigma$. Figure 6 shows the growth rate of unstable sidebands for $KB = 0.3$ as a function of ν and α for a fixed $\epsilon k \bar{A} = 0.13$. First, many new bands of instability now appear, with the main band corresponding to the classical theory of Benjamin & Feir without the long wave. For greater α, the new bands gather more closely toward the main band, while both their width and maximum growth rate increase†. Thus one or more higher harmonics of an unstable

† When this paper was nearly completed we learned that Professors J. Zhang and W. K. Melville had obtained similar results by studying the linearized instability of the steady short wave on an irrotational long wave. In their solution the wave steepnesses of the short and long waves are assumed to be $O(\epsilon)$ and $O(\epsilon^{\frac{1}{2}})$ respectively.

sideband may themselves be unstable, thereby leading the evolution process to much greater complexity.

7. Numerical solution of the envelope equation

Guided by the results of the preceeding section, we now solve numerically the cubic Schrödinger equation (6.11) to examine the later development of a pair of sidebands $e^{\pm i\nu\xi}$ with equal amplitude. We assume the disturbance to be in the main unstable band.

From (6.12) and (6.14), we may deduce at the onset of instability

$$\tilde{\mathscr{A}}(\xi, \phi = 0) = 1 + \tfrac{1}{2}(\tilde{b}\,e^{i\nu\xi} + *) + \tfrac{1}{2}i \int (\tilde{W}e^{i\nu\xi} + *)\,d\xi$$

$$= 1 + \tfrac{1}{2}\tilde{b}\left[1 + \frac{\tilde{W}}{\tilde{b}\nu}\right]e^{i\nu\xi} + \tfrac{1}{2}\tilde{b}*\left[1 - \frac{\tilde{W}*}{\tilde{b}*\nu}\right]e^{-i\nu\xi}. \tag{7.1}$$

It is evident from (6.15a, b) that the complex quantities $\tilde{b}$ and $\tilde{W}$ are always out of phase by $\tfrac{1}{2}\pi$. Thus the ratio $\tilde{W}/\tilde{b}$ is purely imaginary and, for a real $\tilde{b}$, (7.1) may be written as

$$\tilde{\mathscr{A}}(\xi, \phi = 0) = 1 + \tfrac{1}{2}\tilde{b}\left[1 + \frac{\tilde{W}}{\tilde{b}\nu}\right](e^{i\nu\xi} + e^{-i\nu\xi}) = 1 + \epsilon_1\,e^{i\theta_1}\cos\nu\xi, \tag{7.2}$$

which defines ϵ_1 and θ_1. For numerical convenience we shall rescale the horizontal coordinate according to

$$\tilde{\xi} = \nu\xi \tag{7.3}$$

so that the initial sideband has wavelength equal to 2π. After rescaling by (7.3), (6.11) takes the canonical form

$$\frac{\partial\tilde{\mathscr{A}}}{\partial\phi} = -\frac{i\alpha\nu^2}{4}\frac{\partial^2\tilde{\mathscr{A}}}{\partial\tilde{\xi}^2} - i\alpha G\left(\phi; \frac{\epsilon\Omega}{\sigma}\right)|\tilde{\mathscr{A}}|^2\tilde{\mathscr{A}}, \tag{7.4}$$

which contains the parameter ν.

A pseudo-spectral split-step method used by Lo & Mei (1985) for solving a fourth-order Schrödinger equation is used again here. The normalized $\tilde{\mathscr{A}}$ is expressed as a finite Fourier series, defined at N grid point $\tilde{\xi}_j$ in $|\pi, \pi]$:

$$\tilde{\mathscr{A}}(\tilde{\xi}_j, \phi) = \frac{1}{2\pi}\sum_{-N/2}^{N/2}\tilde{\mathscr{A}}_m(\phi)\,e^{im\tilde{\xi}_j}. \tag{7.5}$$

Periodic boundary conditions are imposed.

In all numerical examples to be discussed, we have chosen $\epsilon_1 = 0.1$, while ν and $\psi_0(0)$ are those corresponding to the maximum unstable growth according to the Floquet theory. The steepnesses are kept fixed at $\epsilon k\bar{A} = 0.13$ for the short wave, and $KB = 0.3$ for the long wave. The frequency ratio $\epsilon\Omega/\sigma$, hence α, is allowed to vary within a broad range. All calculations were performed with 64 Fourier harmonics. We shall present, for each α, the time evolution of the short-wave envelope $|\tilde{\mathscr{A}}|$ for 50 long-wave periods. In addition, we present the time evolution of the spectral
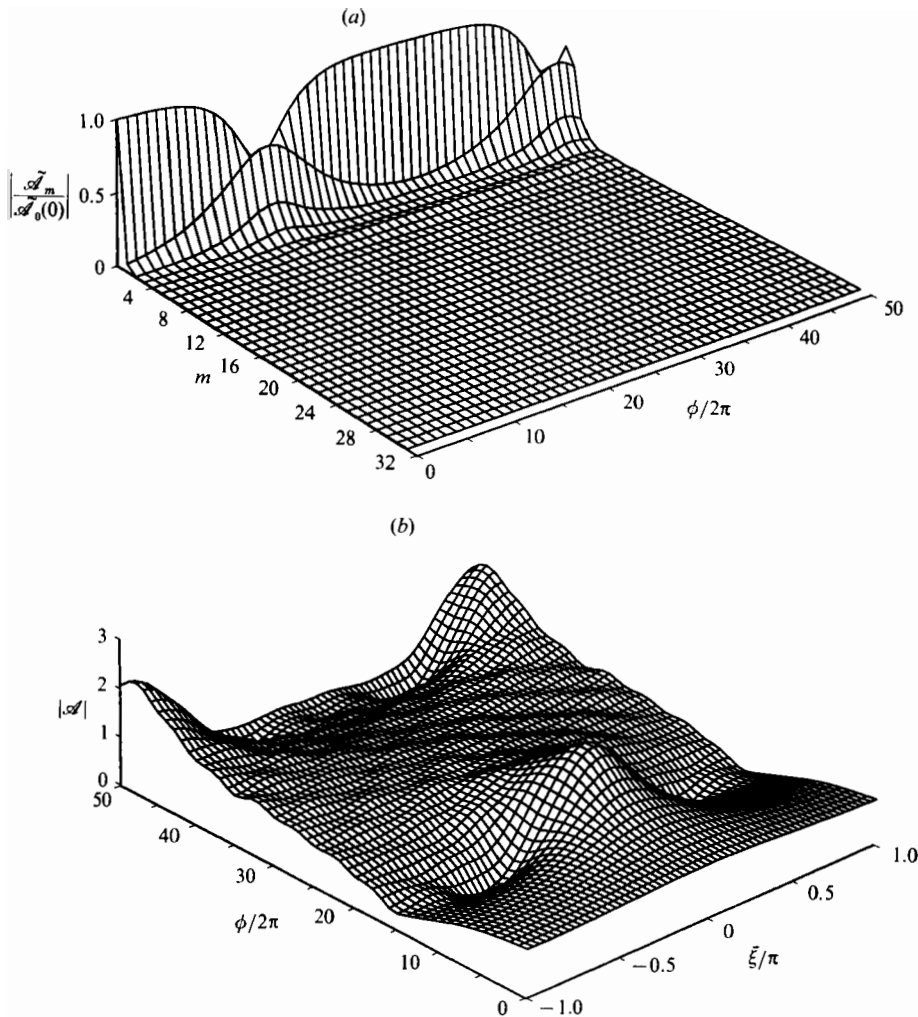
FIGURE 7. Nonlinear evolution of short-wave amplitudes in (a) the Fourier domain, and (b) the physical domain with $KB = 0.3$, $\epsilon k \bar{A} = 0.13$, $\alpha = 0.05$, $\nu = 1.604$ and $\theta_0 = -0.789$.

components, normalized by the initial amplitude of the short Stokes wave. In figures 7(a)–12(a), $m = 0$ corresponds to the short carrier (Stokes) wave, $m = 1$ to the sideband, and $m = 2, 3, \ldots$ to the higher harmonics of the sideband. Note that only those components with positive wavenumbers need to be plotted since the evolution equation (7.4) is symmetric in $\tilde{\xi}$, implying that the Fourier transform is even in m.

First for a small $\alpha = 0.05$, i.e. $\epsilon \Omega / \sigma = 0.1864$, the corresponding maximum growth occurs at $\nu = 1.604$ and $\theta_0(0) = -0.789$ (cf. (7.2)). The envelope evolves in the classical fashion of Fermi–Pasta–Ulam recurrence, as shown in figure 7(a, b). The time series of the Fourier components also show cyclic exchange of energy between the carrier wave and the sideband, whose higher harmonics are carried along passively, see figure 7(a).

For $\alpha = 0.07$ almost-periodic recurrence is still the dominant feature, except that the recurrence wavelength is shortened and less uniform, as shown in figure 8(a, b).

For $\alpha = 0.1$, the envelope evolution is now more complex (figure 9a, b), owing to the fact that the third and fourth harmonics of the principal sideband are now
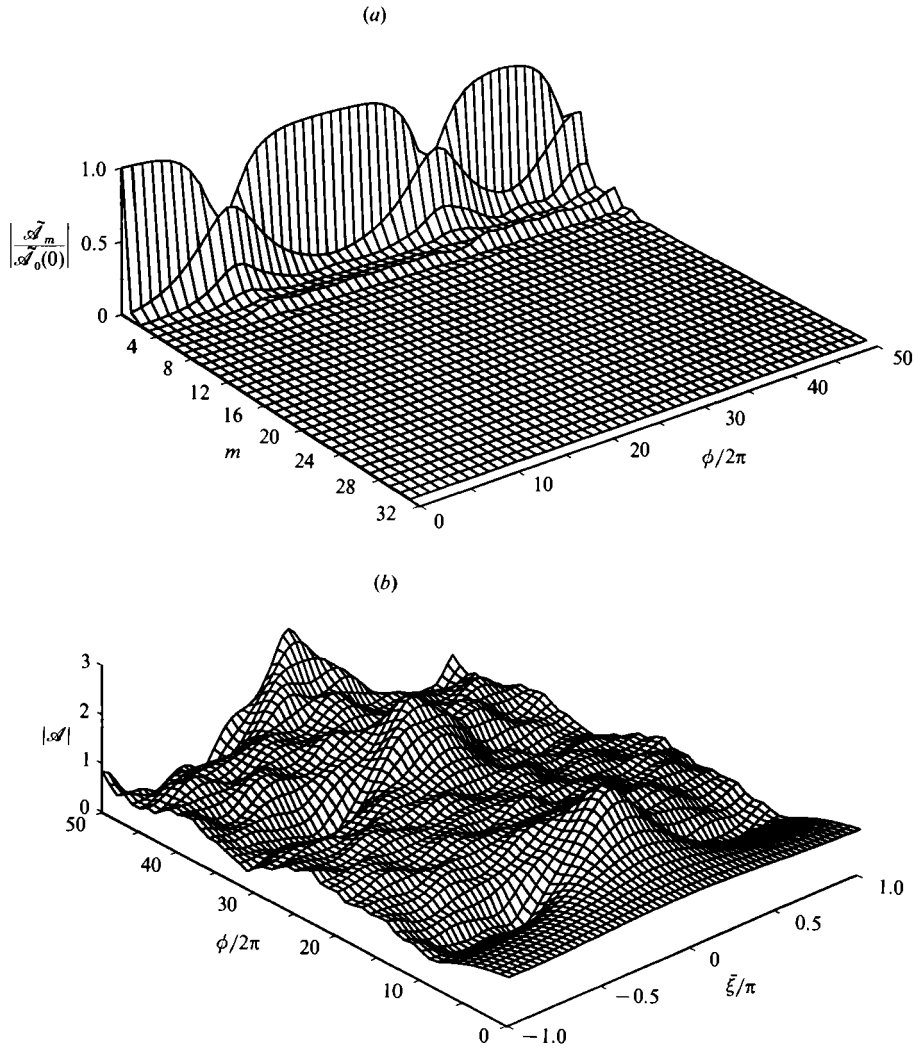
(*a*)

(*b*)

FIGURE 8. As figure 7 but for $\alpha = 0.07$, $\nu = 1.626$ and $\theta_0 = -0.792$.

unstable and take an active role in the nonlinear interaction. The envelope is now becoming irregular in appearance.

When α is increased to 0.125, ($\nu = 1.638$, $\theta_0(0) = -0.8089$ at the maximum growth), the envelope evolution appears more chaotic (figure 10*b*). The spectral time series shows that the total number of active harmonics is still limited (figure 10*a*), therefore the original narrowband assumption is approximately intact.

For $\alpha = 0.15$, energy is exchanged chaotically but now more evenly among the low harmonics, within a somewhat broader band (figures 11*a*, *b*). Finally, as a speculative indication of the trend, numerical results are shown in figures 12 (*a*, *b*) for a relatively large $\alpha = 0.25$ which is somewhat outside the realm of the present asymptotic theory. Chaos is clearly rampant and is accompanied by a broader spectral band.

We have also performed calculations for a milder long wave with $KB = 0.2$, for $\alpha = 0.005$, 0.125 and 0.15 and obtained similar but slightly less dramatic results showing a milder tendency towards apparent chaos with increasing α. This is
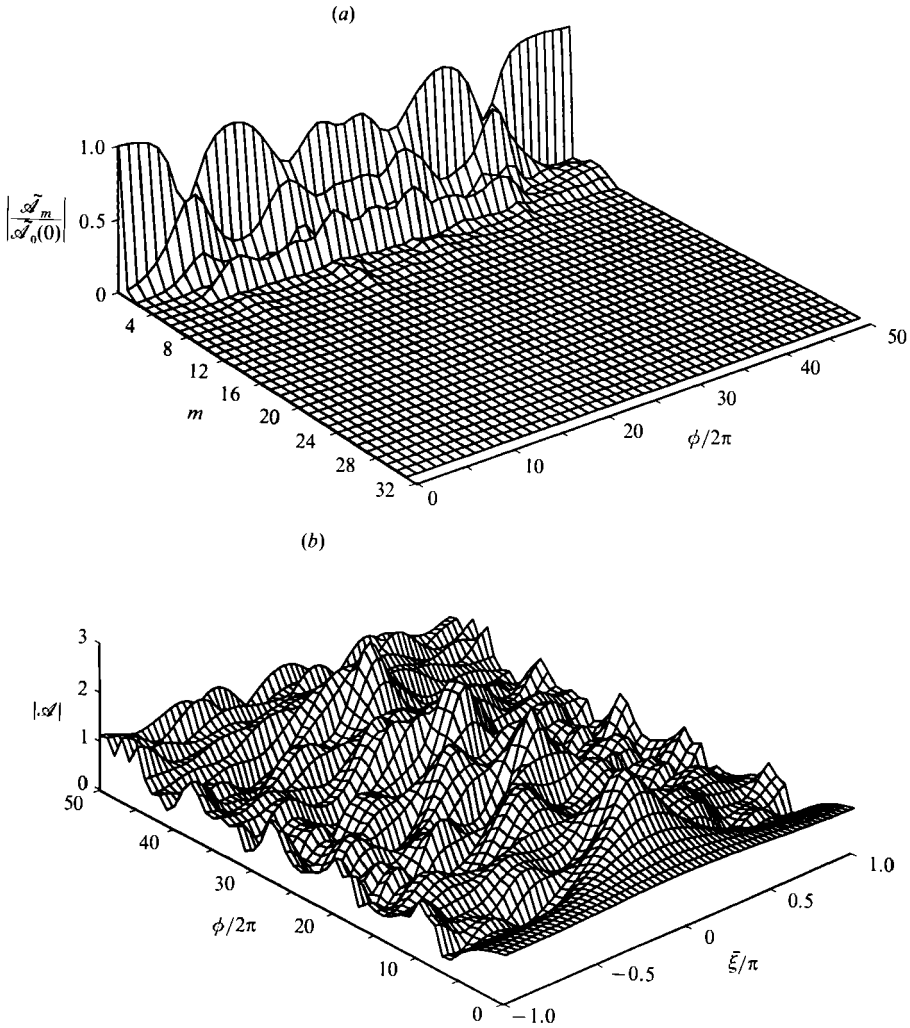
(a)

(b)

FIGURE 9. As figure 7 but for $\alpha = 0.1$, $\nu = 1.637$ and $\theta_0 = -0.80$.

consistent with the fact that the linear growth rate for the sideband depends only weakly on KB, as shown in figure 5.

8. Nonlinear instability of sidebands by a truncated dynamical system

The existence of multiple bands of instability certainly triggers the complex evolution at the initial stage, as one or more higher harmonics of the unstable sideband can also become unstable. To better understand the transition to chaos at the nonlinear stage it is useful to know whether this triggering mechanism is essential. We therefore examine a cruder version of the nonlinear Schrödinger equation by keeping only two active modes in a Fourier series expansion, i.e. the basic Stokes wave and just the pair of unstable sidebands. The resulting approximation is a low-dimensional non-autonomous dynamical system which is much easier to analyse numerically. This kind of truncation has been used successfully before to facilitate analytical examination. For example, to study the
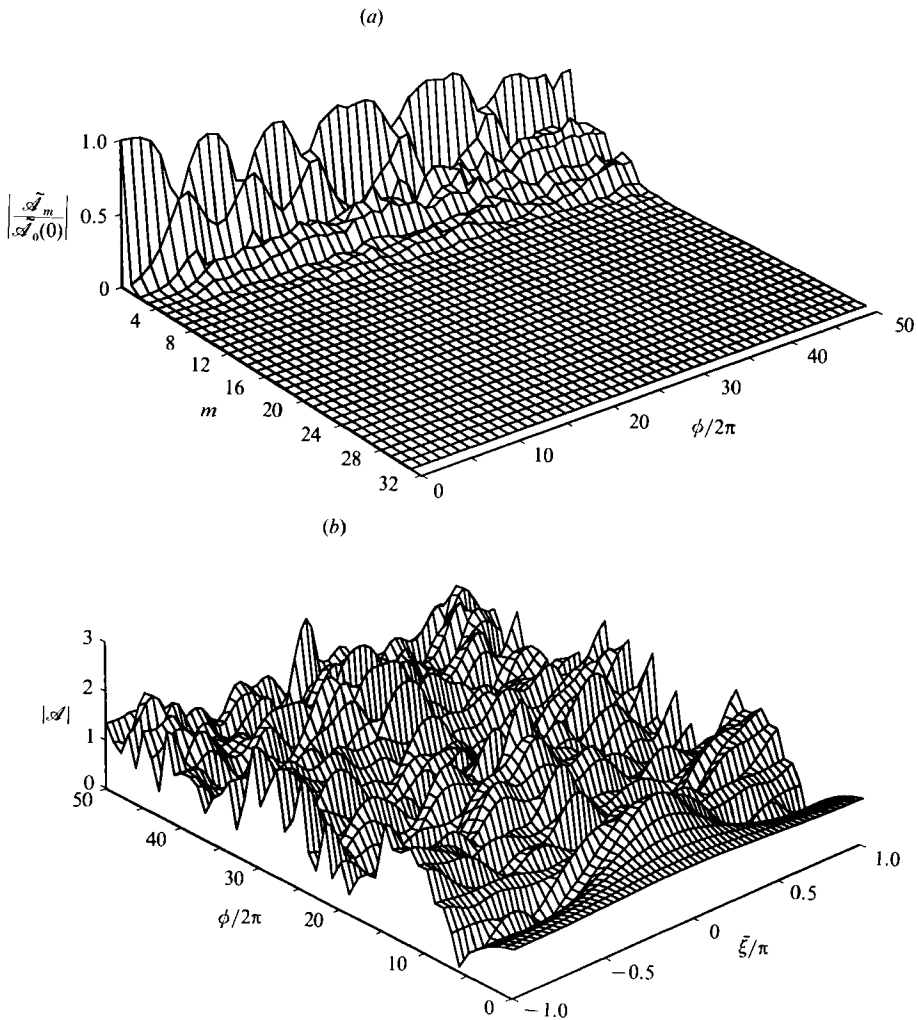
(a)

(b)

FIGURE 10. As figure 7 but for $\alpha = 0.125$, $\nu = 1.639$ and $\theta_0 = -0.8089$.

second harmonic generation in shallow-water waves, Mei & Ünlüata (1973) and Bryant (1973) have reduced the KdV equation to two coupled ordinary differential equations for the first and second harmonics; the recurrence of the second harmonic is then predicted by the celebrated solution of Armstrong *et al.* (1962) in nonlinear optics, and agrees well with experiments. For deep-water waves on an otherwise calm sea surface, Infeld (1981) and Stiassnie & Kroszynski (1982) have shown that by keeping only the Stokes wave and a pair of unstable sidebands, the reduced ordinary differential equations can be solved analytically and yield all the essential nonlinear features of Benjamin–Feir instability. We shall therefore conduct a similar examination.

8.1. *Derivation of the truncated dynamical system*

To follow events subsequent to the initial instability, we assume the following truncated Fourier expansion for $\tilde{\mathscr{A}}(\xi, \phi)$:

$$\tilde{\mathscr{A}} = \tilde{\mathscr{A}}_0 + \frac{1}{\sqrt{2}}\tilde{\mathscr{A}}_1(\mathrm{e}^{\mathrm{i}\nu\xi} + \mathrm{e}^{-\mathrm{i}\nu\xi}), \tag{8.1a}$$
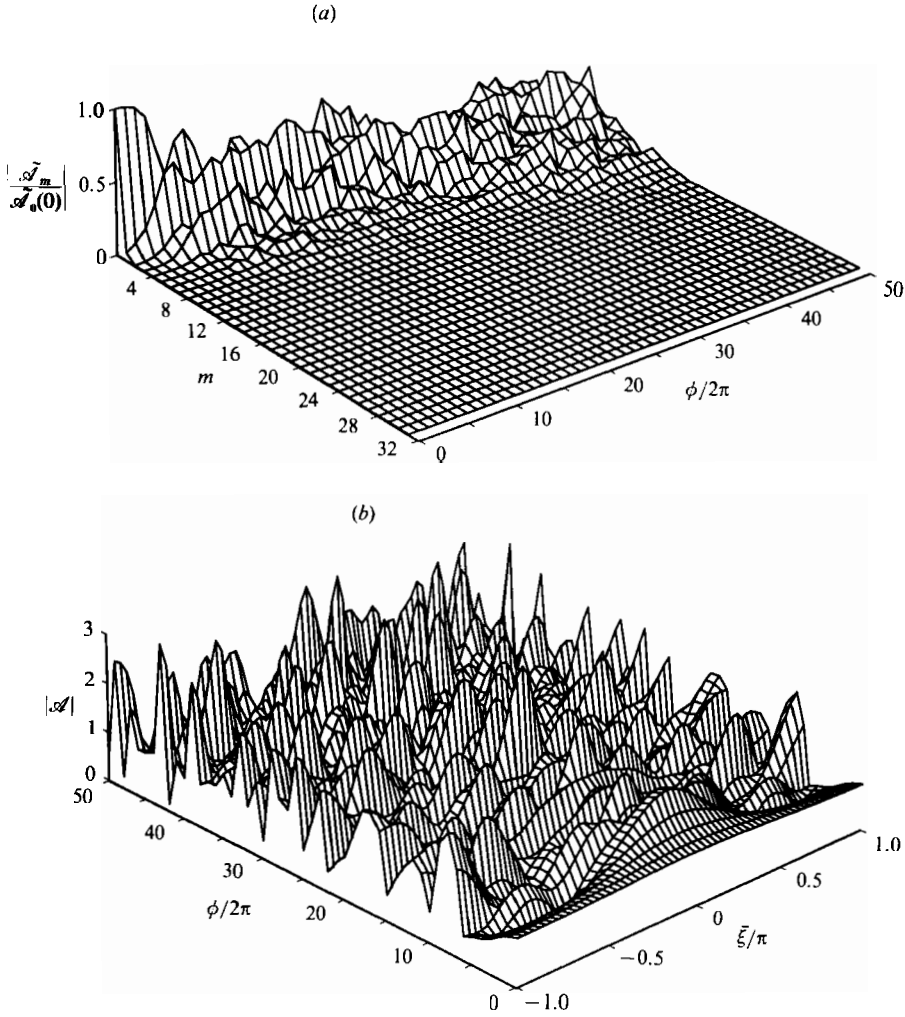
(a)

(b)

FIGURE 11. As figure 7 but for $\alpha = 0.15$, $\nu = 1.638$ and $\theta_0 = -0.817$.

where $\tilde{\mathscr{A}}_0$ and $\tilde{\mathscr{A}}_1$ are respectively the complex amplitudes of the carrier wave and the sideband. They are required to satisfy the initial conditions

$$\tilde{\mathscr{A}}_0(\phi = 0) = 1 \tag{8.2a}$$

and

$$\frac{1}{\sqrt{2}}\tilde{\mathscr{A}}_1(\phi = 0) = \frac{1}{2}\left[\tilde{b} + \frac{\tilde{W}}{\nu}\right] \tag{8.2b}$$

corresponding to the instability theory of Floquet. The factor $1/\sqrt{2}$ is introduced in (8.1) so that the total energy is proportional to $|\tilde{\mathscr{A}}_0|^2 + |\tilde{\mathscr{A}}_1|^2$.

When (8.1) is substituted in (6.11), the cubic term $|\mathscr{A}|^2\mathscr{A}$ becomes

$$|\tilde{\mathscr{A}}_0|^2\,\tilde{\mathscr{A}}_0 + \tilde{\mathscr{A}}_0^*\,\tilde{\mathscr{A}}_1^2 + 2|\tilde{\mathscr{A}}_1|^2\,\tilde{\mathscr{A}}_0$$

$$+ \frac{1}{\sqrt{2}}\{\tilde{\mathscr{A}}_1^*\,\tilde{\mathscr{A}}_0^2 + 2|\tilde{\mathscr{A}}_0|^2\,\tilde{\mathscr{A}}_1 + \tfrac{3}{2}|\tilde{\mathscr{A}}_1|^2\,\tilde{\mathscr{A}}_1\}\{e^{-i\nu\xi} + e^{i\nu\xi}\} + \text{higher harmonics}. \tag{8.3}$$
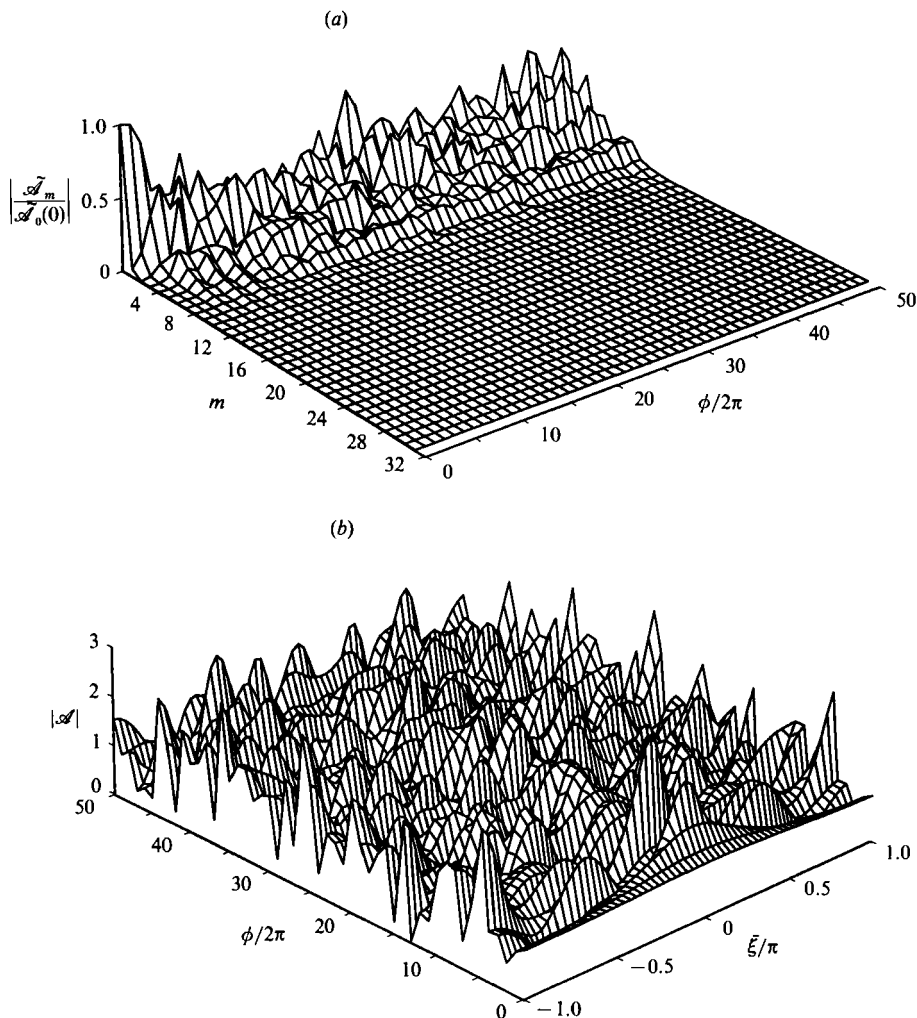
(a)

(b)

FIGURE 12. As figure 7 but for $\alpha = 0.25$, $\nu = 1.615$ and $\theta_0 = -0.865$.

It follows by keeping only two harmonics that

$$\frac{\partial \tilde{\mathscr{A}}_0}{\partial \phi} = -\mathrm{i}\alpha G(\phi)\{|\tilde{\mathscr{A}}_0|^2\,\tilde{\mathscr{A}}_0 + \tilde{\mathscr{A}}_0^*\,\tilde{\mathscr{A}}_1^2 + 2|\tilde{\mathscr{A}}_1|^2\,\tilde{\mathscr{A}}_0\} \qquad (8.4a)$$

and

$$\frac{\partial \tilde{\mathscr{A}}_1}{\partial \phi} = \frac{\mathrm{i}\alpha\nu^2}{4}\,\tilde{\mathscr{A}}_1 - \mathrm{i}\alpha G(\phi)\{\tilde{\mathscr{A}}_1^*\,\tilde{\mathscr{A}}_0^2 + 2|\tilde{\mathscr{A}}_0|^2\,\tilde{\mathscr{A}}_1 + \tfrac{3}{2}|\tilde{\mathscr{A}}_1|^2\,\tilde{\mathscr{A}}_1\} \qquad (8.4b)$$

The parametric dependence of G on $\epsilon\Omega/\sigma$ is suppressed for brevity. These truncated equations couple the two amplitudes $\tilde{\mathscr{A}}_0$ and $\tilde{\mathscr{A}}_1$ nonlinearly.

8.2. *Reduction to Hamiltonian equations*

Next, we introduce the action and angle variables which represent physically the energy and phase of each mode,

$$\tilde{\mathscr{A}}_0 = (2I_0)^{\frac{1}{2}}\mathrm{e}^{\mathrm{i}\theta_0}, \quad \tilde{\mathscr{A}}_1 = (2I_1)^{\frac{1}{2}}\mathrm{e}^{\mathrm{i}\theta_1}. \qquad (8.5)$$

Separating the real from the imaginary parts of $(8.4a, b)$, a non-autonomous dynamical system of the fourth order is obtained:

$$\frac{dI_0}{d\phi} = 4\alpha G(\phi) I_0 I_1 \sin 2(\theta_1 - \theta_0), \qquad (8.6a)$$

$$\frac{d\theta_0}{d\phi} = -\alpha G(\phi) \{2I_0 + 4I_1 + 2I_1 \cos 2(\theta_1 - \theta_0)\}, \qquad (8.6b)$$

$$\frac{dI_1}{d\phi} = -4\alpha G(\phi) I_0 I_1 \sin 2(\theta_1 - \theta_0), \qquad (8.6c)$$

$$\frac{d\theta_1}{d\phi} = \frac{\alpha \nu^2}{4} - \alpha G(\phi) \{4I_0 + 3I_1 + 2I_0 \cos 2(\theta_1 - \theta_0)\}. \qquad (8.6d)$$

They can be expressed as a Hamiltonian system

$$\frac{dI_0}{d\phi} = -\frac{\partial \mathscr{H}}{\partial \theta_0}, \quad \frac{d\theta_0}{d\phi} = \frac{\partial \mathscr{H}}{\partial I_0}, \quad \frac{dI_1}{d\phi} = -\frac{\partial \mathscr{H}}{\partial \theta_1}, \quad \frac{d\theta_1}{d\phi} = \frac{\partial \mathscr{H}}{\partial I_1}, \qquad (8.7a\text{--}d)$$

with the Hamiltonian

$$\mathscr{H}(I_0, \theta_0, I_1, \theta_1, \phi) = \tfrac{1}{4}\alpha\nu^2 I_1 - \alpha G(\phi) \{I_0^2 + \tfrac{3}{2}I_1^2 + 4I_0 I_1 + 2I_0 I_1 \cos 2(\theta_0 - \theta_1)\}. \quad (8.8)$$

Since the angles $\theta_{i,j}$ appear only in the difference form, we introduce the following canonical contact transformation via the generating function F,

$$\psi_0 = \theta_0 - \theta_1, \quad \psi_1 = \theta_0 + \theta_1, \quad F = (\theta_0 - \theta_1) J_0 + (\theta_0 + \theta_1) J_1. \qquad (8.9a\text{--}c)$$

It then follows by definition that

$$I_0 = \frac{\partial F}{\partial \theta_0} = J_1 + J_0, \quad I_1 = \frac{\partial F}{\partial \theta_1} = J_1 - J_0. \qquad (8.10)$$

The Hamiltonian $\mathscr{H}$ may now be expressed in terms of these new variables

$$\mathscr{H}(J_0, \psi_0, J_1, \psi_1, \phi) = \tfrac{1}{4}\alpha\nu^2(J_1 - J_0) + \alpha G(\phi) \{\tfrac{3}{2}J_0^2 + J_0 J_1 - \frac{13}{2}J_1^2 + 2(J_0^2 - J_1^2) \cos 2\psi_0\}, \qquad (8.11)$$

which is cyclic in ψ_1; therefore,

$$\frac{dJ_1}{d\phi} = -\frac{\partial \mathscr{H}}{\partial \psi_1} = 0 \qquad (8.12)$$

and the action variable J_1 is a constant of motion. Since from (8.10),

$$J_0 = \tfrac{1}{2}(I_0 - I_1), \quad J_1 = \tfrac{1}{2}(I_0 + I_1), \qquad (8.13)$$

(8.12) clearly implies energy conservation. Now the contact transformation (8.9) is canonical, hence we may reduce the Hamiltonian equations to

$$\frac{dJ_0}{d\phi} = \dot{J}_0 = -\frac{\partial \mathscr{H}}{\partial \psi_0} = 4\alpha G(\phi) (J_0^2 - J_1^2) \sin 2\psi_0, \qquad (8.14a)$$

$$\frac{d\psi_0}{d\phi} = \dot{\psi}_0 = \frac{\partial \mathscr{H}}{\partial J_0} = -\tfrac{1}{4}\alpha\nu^2 + \alpha G(\phi) \{3J_0 + J_1 + 4J_0 \cos 2\psi_0\}, \qquad (8.14b)$$
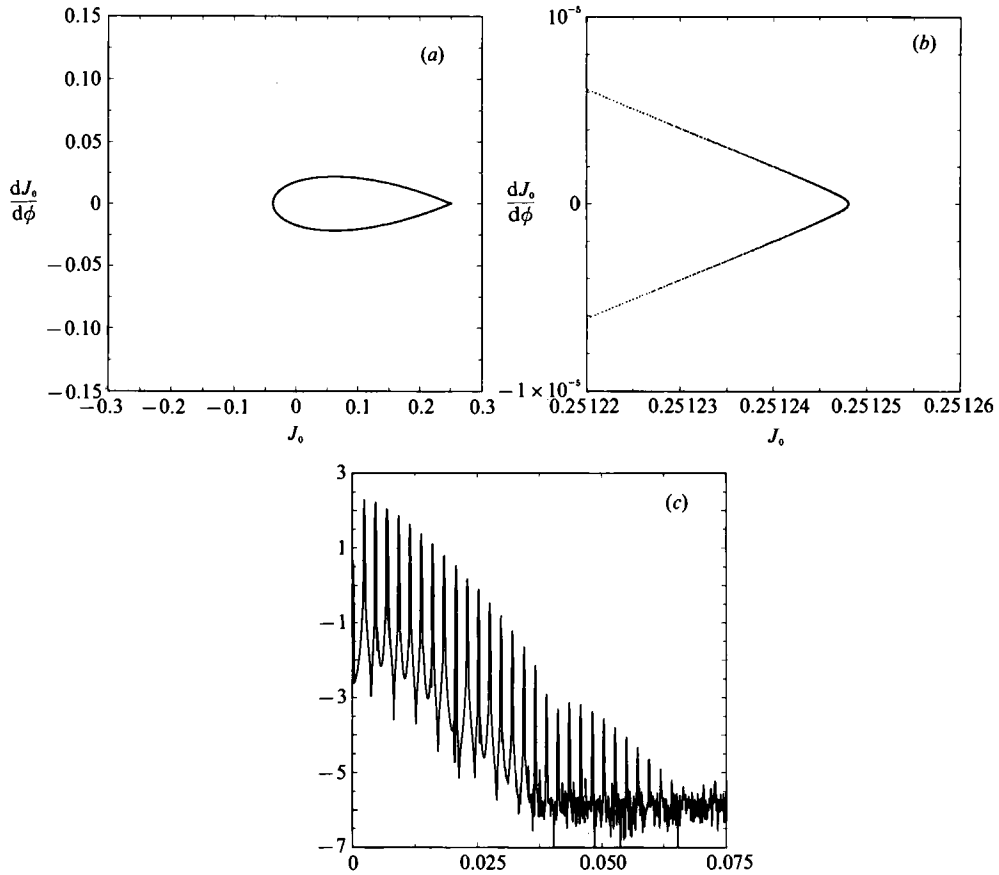
FIGURE 13. (a) Poincaré map in the plane $(J_0, \dot{J}_0)$. (b) Details of the Poincaré map in the vicinity of the corner. (c) Frequency spectrum of J_0 with $KB = 0.3$, $\epsilon k \bar{A} = 0.13$, $\alpha = 0.05$, $\nu_{max} = 1.604$ and $\psi_0(0) = -\theta_1(0) = 0.789$.

which comprise a non-autonomous dynamical system with just two variables, and can easily be examined numerically.

8.3. *Numerical solution*

For a given set of initial data, the Hamiltonian system is integrated numerically by an Adams–Bashforth scheme†. We shall present our results in a Poincaré map by taking stroboscopic projections of a trajectory onto the phase plane of J_0 and $\dot{J}_0$, at the interval of $\Delta\phi = 2\pi$. Thus each phase point coincides with the passage of a long-wave crest. As in §7, we shall analyse the effects of the frequency ratio $\epsilon\Omega/\sigma$ for fixed $\epsilon k \bar{A} = 0.13$ and $KB = 0.3$. The initial conditions are chosen to correspond to the most unstable sideband according to Floquet calculations of §6. In terms of the initial amplitudes, $\tilde{\mathscr{A}}_0 = 1$ and $|\mathscr{A}_1| = \epsilon_1/\sqrt{2}$, the implied initial values of the action and angle variables are

$$I_0 = \tfrac{1}{2}, \quad \theta_0 = 0, \quad (2I_1)^{\frac{1}{2}} = \frac{\epsilon_1}{\sqrt{2}}. \tag{8.15}$$

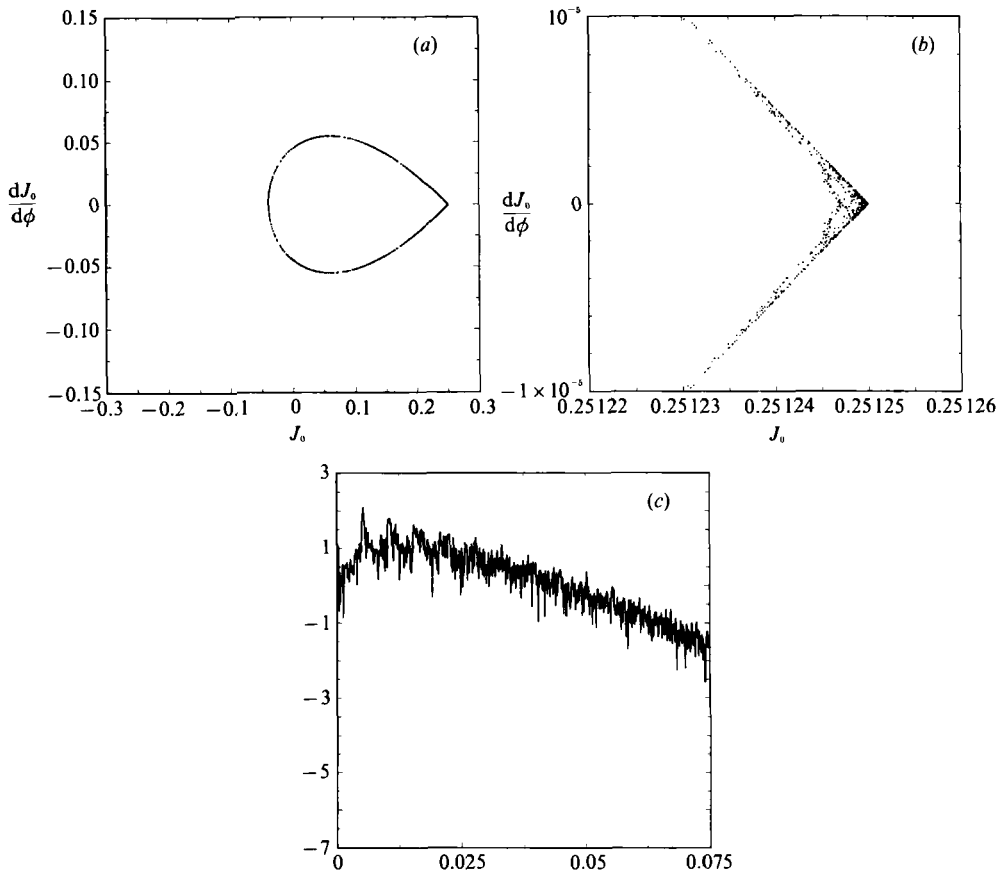† All computations in this section were performed with the commercial software, Dynamical Systems I & II.

FIGURE 14. As figure 13 but for $\alpha = 0.125$, $\nu_{max} = 1.639$ and $\psi_0(0) = -\theta_1(0) = 0.8089$.

The implied values of J_0 and J_1 are in turn derived from (8.13):

$$J_0(\phi = 0) = \tfrac{1}{8}(2 - \epsilon_1^2), \quad J_1(\phi = 0) = \tfrac{1}{8}(2 + \epsilon_1^2). \qquad (8.16\,a, b)$$

From (8.9a), the initial value of ψ_0 is

$$\psi_0(\phi = 0) = -\theta_1(\phi = 0). \qquad (8.17)$$

As in §7, we choose $\epsilon_1 = 0.1$ in all our calculations here and vary $\epsilon\Omega/\sigma$, or equivalently α. Recall from figure 6 that the larger the value of α, the more the unstable the bands and the larger the corresponding maximum growth rate. We shall only consider cases where the higher harmonics of $\mathscr{A}_1$ are either stable or just weakly unstable, in order not to violate seriously the restrictions on our truncated dynamical system.

For a very small value $\alpha = 0.05$ corresponding to figure 7, the second and the third harmonics of $\mathscr{A}_1$ are both linearly stable, while the fourth harmonic is unstable with a Floquet multiplier equal to 1.05. Therefore our dynamical system should yield meaningful results. The Poincaré map consisting of 2500 points falls on a closed curve in the shape of a tear drop, implying a quasi-periodic orbit, see figure 13(a); the magnified portrait of the corner shows a sharply defined curve (figure 13b). The power spectrum of J_0 is characterized by isolated peaks including one at a very low frequency (figure 13c).

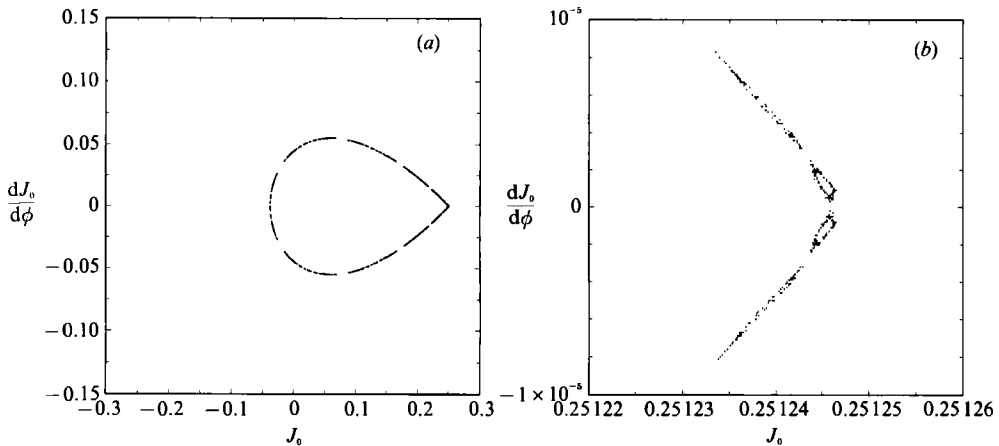We omit the case $\alpha = 0.1$ since the second harmonic of the most unstable sideband

FIGURE 15. (a) Poincaré map in the plane $(J_0, \dot{J}_0)$. (b) Details of Poincaré map in the vicinity of the corner with $KB = 0.3$, $\epsilon k\bar{A} = 0.13$, $\alpha = 0.125$, $\nu_{\max} = 1.639$ and $\psi_0(0) = -\theta_1(0) = 0.808$.
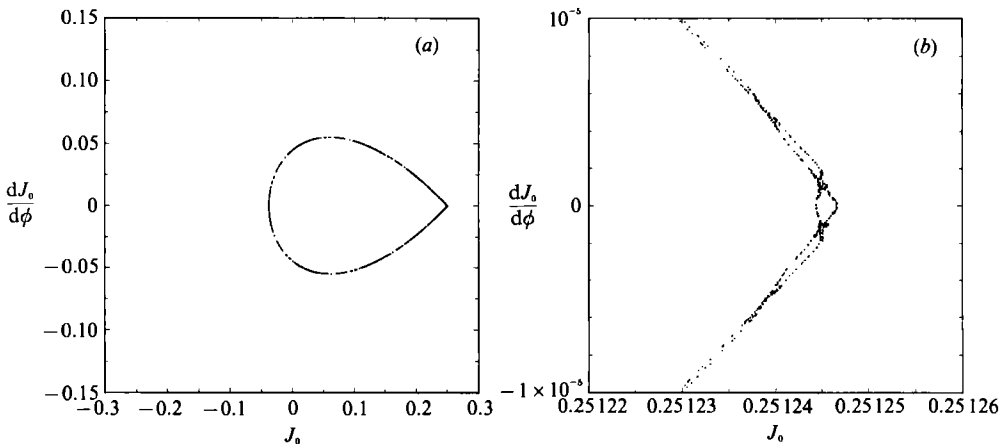

FIGURE 16. As figure 15 but for $\alpha = 0.125$, $\nu_{\max} = 1.639$ and $\psi_0(0) = -\theta_1(0) = 0.8097$.

is also unstable. Consider now $\alpha = 0.125$. Again only the fourth harmonic of $\mathscr{A}_1$ is additionally unstable with a Floquet multiplier equal to 1.11. In the Poincaré map the density of phase points appears to be greater near the corner, see figure 14(a). Upon magnification, phase points are found to splatter near the corner, as seen in figure 14(b). This suggests the onset of chaos, as is confirmed by the flat power spectrum of J_0 shown in figure 14(c).

For the same α, we let the initial phase angle be slightly different from those for the maximum growth. For $\psi_0(0) = 0.8080$, the Poincaré map is now drastically changed to a closed orbit consisting of broken curves, as shown in figure 15(a). Upon magnification of the corner, islands are revealed in figure 15(b). For another value of $\psi_0(0)$, equal to 0.8097, the Poincaré map is shown in figure 16(a). Different islands are seen in the corner neighbourhood after magnification, in figure 16(b). This is evidence that the phase trajectory is sensitive to initial data, and that chaos is not confined to the most unstable state.

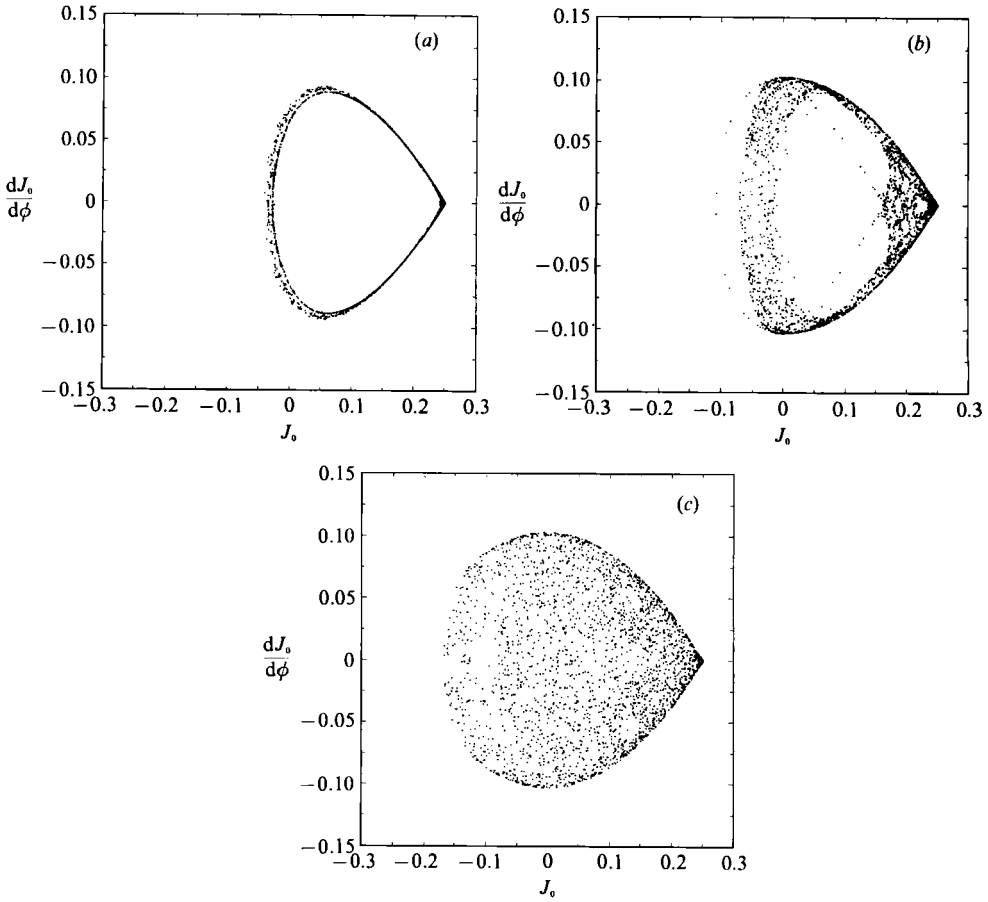With a view to suggesting the possible trend, we now present in figures 17(a)–17(c)

FIGURE 17. Poincaré maps in the plane $(J_0, \dot{J}_0)$ for (a) $\alpha = 0.25$, $\nu = 1.615$ and $\psi_0(0) = 0.865$, (b) $\alpha = 0.3$, $\nu = 1.598$ and $\psi_0(0) = -\theta_1(0) = 0.892$, and (c) $\alpha = 0.45$, $\nu = 1.545$ and $\psi_0(0) = -\theta_1(0) = 0.970$, with $KB = 0.3$, $\epsilon k \bar{A} = 0.13$. The wavenumbers and initial phases correspond to the greatest instability.
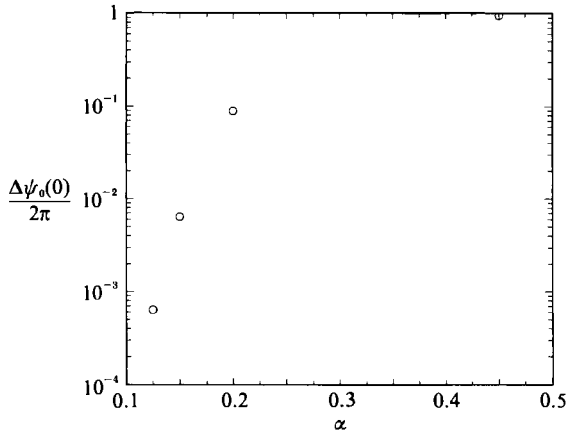

FIGURE 18. Basin of chaos for various parameters α.

results for $\alpha = 0.25$, 0.3 and 0.45, extending beyond the legitimate realm of applicability of the truncated system. The region of chaos in the phase plane expands rapidly with increasing α, and the tear drop is ultimately filled by phase points.

Since chaos can occur when the initial phase parameter does not necessarily coincide with the prediction of the linearized Floquet theory, we have examined the basin of chaos measured by the ratio $\Delta\psi_0(0)/2\pi$, where the numerator represents the union of all initial phase angles leading to chaos (a ratio of 1 means that all values of the initial phase yield chaos). With KB and $\epsilon k\bar{A}$ being fixed as before, figure 18 shows that the ratio so defined increases with α, as expected.

Although all discussions here are for a very steep long wave with $KB = 0.3$, calculations for a milder long wave with $KB = 0.2$ again show qualitatively similar, but slightly less dramatic results, which need not be presented here.

9. Concluding remarks

In this paper we have considered the linear and nonlinear stages of Benjamin–Feir instability of a short gravity wave, subjected to the parametric excitation of a finite-amplitude long wave. Owing to the inherent nonlinearity in the short wave and its nonlinear interaction with the long wave, instability of the short wave can lead to chaotic evolution after a long time. This is shown by a simple model of the long wave which has finite vorticity. This type of mathematical deduction based on the assumption of strictly periodic long waves, with or without vorticity, is of course a mathematical idealization, but it suggests a mechanism that may lead to the irregular appearance of the ocean surface. Precise confirmation by laboratory experiments is expected to be difficult, since to generate two gravity-wave trains with such vastly contrasting scales would require a wavetank of extraordinary length. In nature and in the laboratory there are other instability mechanisms that both the short and long waves are subjected to and that are not accounted for here. Therefore, theoretical extensions of the present work would be desirable in several directions. First of all the slow-modulation assumption here implies narrowbandedness which is not easily upheld because of the multiple bands of instability. A theory based on Zakharov's formalism would be very useful. It is also worthwhile to examine the mechanism of quartet resonance of short waves during the passage of much longer waves. In addition, the effects of capillarity, the unsteadiness of the long wave, the inevitable presence of dissipation with or without breaking in both short and long waves, and the forcing by wind, etc., may all play decisive roles in the complex evolution. In view of its simplicity, Gerstner's exact solution may yet serve as a convenient stepping stone towards the better understanding of some of these important aspects. More numerical investigations based on irrotational long waves are of course also worthwhile.

Appendix A. Governing equations at $O(\epsilon^3)$

Continuity

$$\frac{\partial z_3}{\partial c}+\frac{\partial z_2}{\partial c_1}+\frac{\partial z_1}{\partial c_2}+\frac{\partial x_3}{\partial a}+\frac{\partial x_2}{\partial a_1}+\frac{\partial x_1}{\partial a_2}+\frac{\partial x_1}{\partial a}\frac{\partial z_2}{\partial c}-\frac{\partial x_1}{\partial c}\frac{\partial z_2}{\partial a}+\frac{\partial x_2}{\partial a}\frac{\partial z_1}{\partial c}+\frac{\partial x_1}{\partial a_1}\frac{\partial z_1}{\partial c}-\frac{\partial x_2}{\partial c}\frac{\partial z_1}{\partial a}$$

$$-\frac{\partial x_1}{\partial c_1}\frac{\partial z_1}{\partial a}+\frac{\partial x_1}{\partial a}\frac{\partial z_1}{\partial c_1}-\frac{\partial x_1}{\partial c}\frac{\partial z_1}{\partial a_1}+\frac{\partial x_3}{\partial a}\frac{\partial z_{-2}}{\partial c_2}+\frac{\partial x_2}{\partial a_1}\frac{\partial z_{-2}}{\partial c_2}+\frac{\partial x_1}{\partial a_2}\frac{\partial z_{-2}}{\partial c_2}-\frac{\partial x_3}{\partial c}\frac{\partial z_{-2}}{\partial a_2}-\frac{\partial x_2}{\partial c_1}\frac{\partial z_{-2}}{\partial a_2}$$

$$-\frac{\partial x_1}{\partial c_2}\frac{\partial z_{-2}}{\partial a_2}+\frac{\partial x_{-2}}{\partial a_2}\frac{\partial z_3}{\partial c}-\frac{\partial x_{-2}}{\partial c_2}\frac{\partial z_3}{\partial a}+\frac{\partial x_{-2}}{\partial a_2}\frac{\partial z_2}{\partial c_1}-\frac{\partial x_{-2}}{\partial c_2}\frac{\partial z_2}{\partial a_1}+\frac{\partial x_{-2}}{\partial a_2}\frac{\partial z_1}{\partial c_2}-\frac{\partial x_{-2}}{\partial c_2}\frac{\partial z_1}{\partial a_2}=0;$$

(A 1 a)

Vorticity

$$\frac{\partial^3 x_3}{\partial c\,\partial t^2}+2\frac{\partial^3 x_2}{\partial t_1\,\partial c\,\partial t}+\frac{\partial^3 x_2}{\partial c_1\,\partial t^2}+2\frac{\partial^3 x_1}{\partial t_2\,\partial c\,\partial t}+\frac{\partial^3 x_1}{\partial c_2\,\partial t^2}+\frac{\partial^3 x_1}{\partial t_1^2\,\partial c}+2\frac{\partial^3 x_1}{\partial c_1\,\partial t_1\,\partial t}-\frac{\partial^3 z_3}{\partial a\,\partial t^2}$$

$$-2\frac{\partial^3 z_2}{\partial t_1\,\partial a\,\partial t}-\frac{\partial^3 z_2}{\partial a_1\,\partial t^2}-2\frac{\partial^3 z_1}{\partial t_2\,\partial a\,\partial t}-\frac{\partial^3 z_1}{\partial a_2\,\partial t^2}-\frac{\partial^3 z_1}{\partial t_1^2\,\partial a}-2\frac{\partial^3 z_1}{\partial a_1\,\partial t_1\,\partial t}+\frac{\partial x_1}{\partial a}\frac{\partial^3 x_2}{\partial c\,\partial t^2}$$

$$+\frac{\partial^3 x_1}{\partial c\,\partial t^2}\frac{\partial x_2}{\partial a}+\frac{\partial x_1}{\partial a_1}\frac{\partial^3 x_1}{\partial c\,\partial t^2}+2\frac{\partial^3 x_1}{\partial t_1\,\partial c\,\partial t}\frac{\partial x_1}{\partial a}+\frac{\partial^3 x_1}{\partial c_1\,\partial t^2}\frac{\partial x_1}{\partial a}-\frac{\partial^3 x_1}{\partial a\,\partial t^2}\frac{\partial x_2}{\partial c}-\frac{\partial x_1}{\partial c}\frac{\partial^3 x_2}{\partial a\,\partial t^2}$$

$$-2\frac{\partial^3 x_1}{\partial t_1\,\partial a\,\partial t}\frac{\partial x_1}{\partial c}-\frac{\partial^3 x_1}{\partial a_1\,\partial t^2}\frac{\partial x_1}{\partial c}-\frac{\partial x_1}{\partial c_1}\frac{\partial^3 x_1}{\partial a\,at^2}+\frac{\partial z_1}{\partial a}\frac{\partial^3 z_2}{\partial c\,\partial t^2}+\frac{\partial^3 z_1}{\partial c\,\partial t^2}\frac{\partial z_2}{\partial a}+\frac{\partial^3 z_1}{\partial c_1\,\partial t^2}\frac{\partial z_1}{\partial a}$$

$$+\frac{\partial z_1}{\partial a_1}\frac{\partial^3 z_1}{\partial c\,\partial t^2}+2\frac{\partial^3 z_1}{\partial t_1\,\partial c\,\partial t}\frac{\partial z_1}{\partial a}-\frac{\partial^3 z_1}{\partial a\,\partial t^2}\frac{\partial z_2}{\partial c}-\frac{\partial z_1}{\partial c}\frac{\partial^3 z_2}{\partial a\,\partial t^2}-\frac{\partial z_1}{\partial c_1}\frac{\partial^3 z_1}{\partial a\,\partial t^2}-2\frac{\partial^3 z_1}{\partial t_1\,\partial a\,\partial t}\frac{\partial z_1}{\partial c}$$

$$-\frac{\partial^3 z_1}{\partial a_1\,\partial t^2}\frac{\partial z_1}{\partial c}+\frac{\partial x_1}{\partial a}\frac{\partial^3 x_{-2}}{\partial t_1^2\,\partial c_2}+\frac{\partial^3 x_3}{\partial c\,\partial t^2}\frac{\partial x_{-2}}{\partial a_2}+\frac{\partial^3 x_2}{\partial c_1\,\partial t^2}\frac{\partial x_{-2}}{\partial a_2}+\frac{\partial^3 x_1}{\partial c_2\,\partial t^2}\frac{\partial x_{-2}}{\partial a_2}$$

$$+\frac{\partial^3 x_1}{\partial t_1^2\,\partial c}\frac{\partial x_{-2}}{\partial a_2}-\frac{\partial^3 x_3}{\partial a\,\partial t^2}\frac{\partial x_{-2}}{\partial c_2}-\frac{\partial^3 x_2}{\partial a_1\,\partial t^2}\frac{\partial x_{-2}}{\partial c_2}-\frac{\partial^3 x_1}{\partial a_2\,\partial t^2}\frac{\partial x_{-2}}{\partial c_2}-\frac{\partial^3 x_1}{\partial t_1^2\,\partial a}\frac{\partial x_{-2}}{\partial c_2}-\frac{\partial x_1}{\partial c}\frac{\partial^3 x_{-2}}{\partial t_1^2\,\partial a_2}$$

$$+2\frac{\partial^3 x_2}{\partial t_1\,\partial c\,\partial t}\frac{\partial x_{-2}}{\partial a_2}+2\frac{\partial^3 x_1}{\partial t_2\,\partial c\,\partial t}\frac{\partial x_{-2}}{\partial a_2}+2\frac{\partial^3 x_1}{\partial c_1\,\partial t_1\,\partial t}\frac{\partial x_{-2}}{\partial a_2}-2\frac{\partial^3 x_2}{\partial t_1\,\partial a\,\partial t}\frac{\partial x_{-2}}{\partial c_2}$$

$$-2\frac{\partial^3 x_1}{\partial t_2\,\partial a\,\partial t}\frac{\partial x_{-2}}{\partial c_2}-2\frac{\partial^3 x_1}{\partial a_1\,\partial t_1\,\partial t}\frac{\partial x_{-2}}{\partial c_2}+\frac{\partial z_1}{\partial a}\frac{\partial^3 z_{-2}}{\partial t_1^2\,\partial c_2}+\frac{\partial^3 z_3}{\partial c\,\partial t^2}\frac{\partial z_{-2}}{\partial a_2}+\frac{\partial^3 z_2}{\partial c_1\,\partial t^2}\frac{\partial z_{-2}}{\partial a_2}$$

$$+\frac{\partial^3 z_1}{\partial c_2\,\partial t^2}\frac{\partial z_{-2}}{\partial a_2}+\frac{\partial^3 z_1}{\partial t_1^2\,\partial c}\frac{\partial z_{-2}}{\partial a_2}-\frac{\partial^3 z_3}{\partial a\,\partial t^2}\frac{\partial z_{-2}}{\partial c_2}-\frac{\partial^3 z_2}{\partial a_1\,\partial t^2}\frac{\partial z_{-2}}{\partial c_2}-\frac{\partial^3 z_1}{\partial a_2\,\partial t^2}\frac{\partial z_{-2}}{\partial c_2}-\frac{\partial^3 z_1}{\partial t_1^2\,\partial a}\frac{\partial z_{-2}}{\partial c_2}$$

$$-\frac{\partial z_1}{\partial c}\frac{\partial^3 z_{-2}}{\partial t_1^2\,\partial a_2}+2\frac{\partial^3 z_2}{\partial t_1\,\partial c\,\partial t}\frac{\partial z_{-2}}{\partial a_2}+2\frac{\partial^3 z_1}{\partial t_2\,\partial c\,\partial t}\frac{\partial z_{-2}}{\partial a_2}+2\frac{\partial^3 z_1}{\partial c_1\,\partial t_1\,\partial t}\frac{\partial z_{-2}}{\partial a_2}$$

$$-2\frac{\partial^3 z_2}{\partial t_1\,\partial a\,\partial t}\frac{\partial z_{-2}}{\partial c_2}-2\frac{\partial^3 z_1}{\partial t_2\,\partial a\,\partial t}\frac{\partial z_{-2}}{\partial c_2}-2\frac{\partial^3 z_1}{\partial a_1\,\partial t_1\,\partial t}\frac{\partial z_{-2}}{\partial c_2}=0;$$

(A 1 b)

Free-surface boundary condition

$$\frac{\partial^2 x_3}{\partial t^2} + 2\frac{\partial^2 x_2}{\partial t_1 \partial t} + \frac{\partial^2 x_1}{\partial t_1^2} + 2\frac{\partial^2 x_1}{\partial t_2 \partial t} + g\frac{\partial z_3}{\partial a} + g\frac{\partial z_2}{\partial a_1} + g\frac{\partial z_1}{\partial a_2}$$

$$+\frac{\partial x_1}{\partial a}\frac{\partial^2 x_2}{\partial t^2} + \frac{\partial^2 x_1}{\partial t^2}\frac{\partial x_2}{\partial a} + \frac{\partial x_1}{\partial a_1}\frac{\partial^2 x_1}{\partial t^2} + 2\frac{\partial^2 x_1}{\partial t_1 \partial t}\frac{\partial x_1}{\partial a}$$

$$+\frac{\partial z_1}{\partial a}\frac{\partial^2 z_2}{\partial t^2} + \frac{\partial^2 z_1}{\partial t^2}\frac{\partial z_2}{\partial a} + \frac{\partial z_1}{\partial a_1}\frac{\partial^2 z_1}{\partial t^2} + 2\frac{\partial^2 z_1}{\partial t_1 \partial t}\frac{\partial z_1}{\partial a}$$

$$+\frac{\partial^2 x_3}{\partial t^2}\frac{\partial x_{-2}}{\partial a_2} + \frac{\partial x_3}{\partial a}\frac{\partial^2 x_{-2}}{\partial t_1^2} + \frac{\partial x_2}{\partial a_1}\frac{\partial^2 x_{-2}}{\partial t_1^2} + \frac{\partial^2 x_1}{\partial t_1^2}\frac{\partial x_{-2}}{\partial a_2} + \frac{\partial x_1}{\partial a_2}\frac{\partial^2 x_{-2}}{\partial t_1^2}$$

$$+\frac{\partial^2 z_3}{\partial t^2}\frac{\partial z_{-2}}{\partial a_2} + \frac{\partial z_3}{\partial a}\frac{\partial^2 z_{-2}}{\partial t_1^2} + \frac{\partial z_2}{\partial a_1}\frac{\partial^2 z_{-2}}{\partial t_1^2} + \frac{\partial^2 z_1}{\partial t_1^2}\frac{\partial z_{-2}}{\partial a_2} + \frac{\partial z_1}{\partial a_2}\frac{\partial^2 z_{-2}}{\partial t_1^2}$$

$$+2\frac{\partial^2 x_2}{\partial t_1 \partial t}\frac{\partial x_{-2}}{\partial a_2} + 2\frac{\partial^2 x_1}{\partial t_2 \partial t}\frac{\partial x_{-2}}{\partial a_2} + 2\frac{\partial^2 z_2}{\partial t_1 \partial t}\frac{\partial z_{-2}}{\partial a_2} + 2\frac{\partial^2 z_1}{\partial t_2 \partial t}\frac{\partial z_{-2}}{\partial a_2} = 0, \quad c = 0. \quad \text{(A 1 c)}$$

Appendix B. Zero-crossings of the Stokes wave

Following the notation of Schwartz (1974), the free-surface elevation of a deep-water Stokes wave is given parametrically by

$$y(\chi) = a_1 \cos\chi + \tfrac{1}{2}a_2 \cos 2\chi + \ldots + \frac{a_n}{n}\cos n\chi + \ldots, \quad \text{(B 1 a)}$$

$$-x(\chi) = \chi + a_1 \sin\chi + \tfrac{1}{2}a_2 \sin 2\chi + \ldots + \frac{a_n}{n}\sin n\chi + \ldots, \quad \text{(B 1 b)}$$

where χ represents the Eulerian phase (ϕ_E in this paper) along the Stokes wave profile and the a_j are expressed in powers series of the slope h (KB in this paper) as follows:

$$\left.\begin{aligned}a_1 &= h - \tfrac{3}{2}h^3 - \tfrac{1}{24}h^5 + O(h^7), \quad a_2 = 2h^3 - 5h^4 + \tfrac{19}{6}h^6 + O(h^8),\\ a_3 &= \tfrac{9}{2}h^3 - \tfrac{31}{2}h^5 + O(h^7), \quad a_4 = \tfrac{32}{3}h^4 - \tfrac{839}{18}h^6 + O(h^8),\\ a_5 &= \tfrac{625}{24}h^5 + O(h^7), \quad a_6 = \tfrac{324}{5}h^6 + O(h^8).\end{aligned}\right\} \quad \text{(B 2)}$$

The mean surface elevation $\bar{y}$ is also given in power series of h by

$$\bar{y} = \tfrac{1}{2}h^2 - \tfrac{1}{2}h^4 - \tfrac{13}{24}h^6 + O(h^8). \quad \text{(B 3)}$$

The zero-crossings χ_{crossing} are solutions of

$$y(\chi) = \bar{y}. \quad \text{(B 4)}$$

In the interval $[0, 2\pi]$, (B 4) admits two solutions in the vicinity of $\tfrac{1}{2}\pi$ and $\tfrac{3}{2}\pi$. By symmetry, it is sufficient to examine only the vicinity of $\tfrac{1}{2}\pi$ and let

$$\chi_{\text{crossing}} = \tfrac{1}{2}\pi + \sum_{i=1}^{5} p_i h^i. \quad \text{(B 5)}$$

Substitution of (B 5) in (B 4) with the help of (B 2) and (B 3) yields the values of p_i and

$$\chi_{\text{crossing}} = \tfrac{1}{2}\pi - \tfrac{3}{2}h + \tfrac{29}{48}h^3 + \tfrac{5743}{11520}h^5 + O(h^7). \quad \text{(B 6)}$$

In our notation, $\chi = \phi_E$ and $h = KB$.

REFERENCES

ARMSTRONG, J. A., BLOEMBERGEN, N., DUCUING, J. & PERSHAN, P. S. 1962 Interactions between light waves in a nonlinear dielectric. *Phys. Rev.* **127**, 1818–1939.

BENJAMIN, T. B. & FEIR, J. E. 1967 The disintegration of wave trains on deep water. *J. Fluid Mech.* **27**, 417–430.

BRETHERTON, F. P. & GARRETT, C. J. R. 1969 Wavetrains in inhomogeneous moving media. *Proc. R. Soc. Lond.* A **302**, 529–544.

BRYANT, P. J. 1973 Periodic waves in shallow water. *J. Fluid Mech.* **59**, 625–644.

GERSTNER, F. J. VON 1802 Theorie der wellen. *Abh. k. böhm. Ges. Wiss.*

HENYEY, F. S., CREAMER, D. B., DYSTHE, K., SCHULT, R. L. & WRIGHT, J. A. 1988 The energy and action of small waves riding on large waves. *J. Fluid Mech.* **189**, 443–462.

INFELD, E. 1981 Quantitative theory of the Fermi–Pasta–Ulam recurrence in the nonlinear Schrödinger equation. *Phy. Rev. Lett.* **47**, 717–718.

IOOSS, G. & JOSEPH, D. D. 1980 *Elementary Stability and Bifurcation Theory*. Springer.

KHARIF, C. 1990 Some aspects of the kinematics of short waves over longer gravity waves on deep water. In *Water Wave Kinematics* (ed. A. Tørum), pp. 265–279. Klumer.

KOCHIN, N. E., KIBEL, I. A. & ROZE, N. V. 1965 *Theoretical Hydrodynamics*, 2nd edn. Interscience.

LO, E. & MEI, C. C. 1985 A numerical study of water-wave modulation based on a higher-order nonlinear Schröinger equation. *J. Fluid Mech.* **150**, 395–416.

LONGUET-HIGGINS, M. S. 1987 The propagation of short surface waves on longer gravity waves. *J. Fluid Mech.* **177**, 293–306.

LONGUET-HIGGINS, M. S. & STEWART, R. W. 1960 Changes in the form of short gravity waves on long waves and tidal currents. *J. Fluid Mech.* **8**, 566–583.

MEI, C. C. & ÜNLÜATA, Ü. 1973 Harmonic generation in shallow water waves. In *Waves on Beaches* (ed. R. E. Meyer), pp. 181–202. Academic.

NAYFEH, A. H. & MOOK, D. T. 1979 *Nonlinear Oscillations*. Wiley-Interscience.

SCHWARTZ, L. W. 1974 Computer extension and analytic continuation of Stokes expansion for gravity waves. *J. Fluid Mech.* **62**, 553–578.

STIASSNIE, M. & KROSZYNSKI, U. I. 1982 Long-time evolution of an unstable water-wave train. *J. Fluid Mech.* **116**, 207–225.

ZHANG, J. & MELVILLE, W. K. 1990 Evolution of weakly nonlinear short waves riding on long gravity waves. *J. Fluid Mech.* **214**, 321–346.